TÉCNICO LISBOA

Numerical Simulation of Newtonian Fluid Mixing Inside Asymmetric T-Shaped Micromixers

Tiago Miguel Saldanha António

Thesis to obtain the Master of Science Degree in

Mechanical Engineering

Supervisors: Prof. Viriato Sérgio de Almeida Semião

Prof. Aires José Pinto dos Santos

Examination Committee

Chairperson: Prof. Carlos Frederico Neves Bettencourt da Silva

Supervisor: Prof. Viriato Sérgio de Almeida Semião

Member of the Commitee: Prof. Miguel Abreu de Almeida Mendes

June 2019

Acknowledgements

I would like to give my special thanks to my two supervisors, Prof. Aires and Prof. Viriato, for the patience demonstrated when I wasn't able to show work at the desirable rate. It was also remarkable their help with the physical analysis of the flows.

I also want to thank Fnac Portugal, LFP-Lojas Francas de Portugal, Bosch Service Solutions and BMW Group Portugal, as my employers. I never had to fail an exam or test being scheduled to work. I need to highlight Bosch and BMW, for recognising in me the skills needed to work in such a competitive and demanding field as the Automotive.

Thank you Célia Gonçalves for your precious help setting up the references of this work! It is probably the most boring part, so the sushi dinner you asked is more than deserved.

Last but not the least I give the biggest acknowledgement to my family. Everyone took this journey with me, were there to share the victories and, most importantly, my defeats. There was times where I though I would never get the opportunity to write these letters in this document. You never let me give up, so this Master Thesis is also yours.

Avô Ramiro e Tio Jorge, espero que onde quer que estejam sintam orgulho por ter conseguido chegar ao fim desta jornada. Outras seguem-se.

Abstract

Achieving efficient mixing of flow streams is one of the important challenges of microfluidics, because of the difficulty to induce flow transition to the turbulent regime. Of the different solutions for devices proposed, T-shaped micromixers stand out, as they have a simple geometry and low production cost and showed promising results when asymmetric inlet conditions are applied. Starting from experimental results obtained when equal flow rates were applied to inlets with different widths, four geometries (one symmetric and three asymmetric) were modelled using CAD 3D software Solidworks. Then, the numerical simulation of twelve flows, corresponding to the Reynolds number based on the outlet channel range of 25 to 295, inside each model was performed. This tool allowed the understanding of how the degree of asymmetry influence mixing quality, and the physical characterization of the five flow regimes previously identified. This allowed to conclude that increasing asymmetry favours mixing quality and also that after transition to *engulfment* regime, symmetrical micromixers perform better than asymmetrical ones.

Keywords: Microfluids; T-shaped Micromixers; Mixing; Numerical Simulation

Resumo

A obtenção de misturas de escoamentos o mais eficientes possível é um dos maiores desafios do campo dos microfluidos, devido à dificuldade na obtenção de escoamentos turbulentos. Dos tipos de micromisturadores existentes, destacam-se os micromisturadores em forma de T, devido ao seu baixo custo de fabrico e desempenho promissor na obtenção de níveis de qualidade de mistura aceitáveis, quando são impostas condições assimétricas de escoamento às suas entradas. Partindo de resultados experimentais de escoamentos onde foram aplicados caudais iguais a entradas de larguras diferentes, modelaram-se quatro micromisturadores (uma simétrica e três assimétricas) utilizando o *software* de CAD 3D *Solidworks*, e procedeu-se à simulação numérica de doze escoamentos no interior das geometrias para números de Reynolds entre 25 e 295. Esta ferramenta permitiu compreender de que forma o grau de assimetria influencia a qualidade de mistura no interior, e também a análise física das estruturas do escoamento presentes nos cinco regimes identificados. Com este trabalho, foi possível caracterizar detalhadamente os cinco regimes de escoamento identificados anteriormente para micromisturadores assimétricos, concluiu-se que o aumento de assimetria favorece a qualidade da mistura e que após a transição para o regime *engulfment* os misturadores simétricos apresentam um melhor desempenho face aos assimétricos.

Palavras-Chave: Microfluidica; Micromisturadores T; Mistura; Simulação Numérica

Contents

Acknowledgements ..... **iii**

Abstract ..... **v**

Resumo ..... **vii**

List of Figures ..... **xii**

List of Tables ..... **xv**

Nomenclature ..... **xvii**

Abreviations xvii

Greek Symbols xvii

Roman Symbols xvii

Subscripts xix

Chapter 1- Introduction **1**

1.1 Motivation 1

1.2 State-of-the-art 2

1.2.1 Internal Flows 2

1.2.2. Fluid Mixing 3

1.2.3. Mixing Inside Microchannels 4

1.2.4. Micromixers 4

1.2.5 T-Micromixers 7

1.2.6. Mixing Quality 10

1.2.7. Effect of Inlet Parameters on the Performance of T-Micromixers 11

1.3 Objectives and Main Contributions of this thesis 14

1.4 Thesis Structure 15

Chapter 2- Numerical Modelling **16**

2.1 The studied T-micromixer geometries 16

2.2 Governing Equations 16

2.3 Numerical Technique 18

2.3.1 The Computational Mesh 19

2.3.2 Spatial Discretization 20

2.3.3 Temporal Discretization 21

2.4 The Studied Case 22
2.4.1 Geometries modelled 23
2.4.2 The Computational Mesh 23
2.4.3 Initial and Boundary Conditions 24
2.4.4 Convergence criteria 25
2.4.5 Grid Convergence Study 25
2.4.6 Data Post-Processing 30
Chapter 3- Presentation and Discussion of Results 31
3.1 The symmetrical case 33
3.2 The Asymmetrical Micromixers 37
3.2.1 Effect of the Reynolds number and flow regimes 37
3.2.2. Effect of the Degree of Asymmetry 44
Chapter 4- Conclusions and Suggestions for Future Work 48
4.1 Conclusions 48
4.2 Suggestions for Future Work 51
References 52
Appendix 55
Additional images of the flows inside the modelled micromixers 55

List of Figures

Figure 1. 1 A LOC device for food allergies detection [5] 1
Figure 1. 2 A LOC device for food allergies detection [5] 1
Figure 1. 3 Classification of different types of micromixers [20] 5
Figure 1. 4 SAR micromixers. (a) Join-split-join, (b) split-join, (c) split-split-join, (d) multiple intersecting [20] .....
Figure 1. 5 A multi-lamination micromixer [14] .....
Figure 1. 6 A zig-zag micromixer [7] .....
Figure 1. 7 A T-shaped micromixer [17] .....
Figure 1. 8 A connected-groove micromixer [7] .....
Figure 1. 9 Representation of a T-micromixer of dimensions $\mathrm{Wi} \times \mathrm{Wo} \times \mathrm{H}$ .....
Figure 1. 10 Schematic based on numerical results of the three steady flow regimes. a) stratified regime for Re=0.1, b) vortex regime for Re=130 and c) engulfment regime for Re=200 9
Figure 1. 11 Quasi-Periodic Pulsating flow regime at Re=390 [30] .....
Figure 1. 12 Periodic pulsating flow at Re=290 [30] .....
Figure 1. 13 Flow visualization of a) regime I (Reo=50), b) regime III (Reo=100), c) regime IV (Reo=222), d) regime V(Reo=289) [23] 13
Figure 2. 1 Representation of the most asymmetric micromixer A3 and the computational domain used. The latter is the volume enclosed by the parallelepiped represented exterior space does not participate in the numerical simulation. .....
Figure 2. 2 Example of a mesh near the solid-fluid interface [17] .....
Figure 2. 3 A typical cell. Capital letters represent neighbouring cells and small letters the cell faces [20]. .....
Figure 2. 4 CAD models of the micromixers. a) General 3D view of the micromixer A1 b), c), d), e) top views of longitudinal cross-sections of micromixers A1, S1, A2 and A3 22
Figure 2. 5 Computational mesh. a) General view. b) A close-up view of the mixing zone of the A3 geometry 23
Figure 2. 6 Representation of the velocity profile at both inlet streams for a Poiseuille flow inside a rectangular cross-section channel [16] .....
Figure 2. 7 Representation of the velocity profile at both inlet streams for a Poiseuille flow inside a rectangular cross-section channel [16] .....
Figure 2. 7 Plot of Log(E) versus Log(h). Modules have been taken because E and h are lower than one .....
Figure 2. 8 Example of exported images and plots exported from SolidWorks Flow Simulation. a) flow visualisation, b) water mass fraction in the middle plane of the micromixers, c) water mass fraction in a plane at 40 μm distant from the middle plane of the micromixers, d) concentration in a cross section located at a distance from the common wall equal to 1057μm. 30

Figure 3. 1 Mixing quality α_mix as a function of the Reynolds number (Re) for the mixers S1 (black circles), S2 (yellow triangles), A1 (green squares with red cross), A2 (red diamonds) and A3 (yellow squares with black lining) .....
Figure 3. 2 Images representative of the three identified regimes for the flow inside the micromixer S1 34
Figure 3. 3 Aditional representations of the flow inside micromixer S1 at Re=250 35
Figure 3. 4 Images for the flow inside a symmetrical micromixer similar to the one modelled (S1). a) and b) stand for Re=140 and Re=156, respectively [2]. 36
Figure 3. 5 Similar work [34]. a) flow streamlines and tubes for Re=12, Re=80 and Re=240. b) α plot as a function of Re for two different values of diffusion coeficient (D=2×10^(-7) m^2/s for the squares and D=1×10^(-6) m^2/s for the diamonds) 37
Figure 3. 6 Representative images of the flow inside micromixer A3, the most asymmetrical, at Re = 25 38
Figure 3. 7 Representative images of the flow inside micromixer A3, the most asymmetrical, at Re=75 39
Figure 3. 8 Representative images of the flow inside micromixer A3, the most asymmetrical, at Re=125 40
Figure 3. 9 Representative images of the flow inside micromixer A3, the most asymmetrical, at Re=200 41
Figure 3. 10 Representative images of the flow inside micromixer A3, the most asymmetrical, at Re=275 44
Figure 3. 11 Plot of the mixing quality versus the kinetic energy rate at the micromixer inlets for the five studied geometries .....
Figure 3. 12 Images of the flow inside micromixer A1, the least asymmetrical, at Re=275 47
Figure A 1. Images of the flow inside A1 at Re=25 55
Figure A 2. Images of the flow inside A1 at Re=75 56
Figure A 3. Images of the flow inside A1 at Re=125 57
Figure A 4. Images of the flow inside A1 at Re=200 58
Figure A 5. Images of the flow inside A2 at Re=25 59
Figure A 6. Images of the flow inside A2 at Re=75 60
Figure A 7. Images of the flow inside A2 at Re=125 61
Figure A 8. Images of the flow inside A2 at Re=200 62
Figure A 9. Images of the flow inside A2 at Re=270 63

List of Tables

Table 1. 1 Typical times for mixing processes with a characteristic length of 100μm [15,16] 4
Table 2. 1 Geometrical characteristics of the micromixers modelled 16
Table 2. 2 Evolution of αmix with h (characteristic grid spacing parameter) for the numerical simulations performed 26
Table 2. 3 Analysis of the Grid Convergence Index for the studied meshes $GCIij = Fs\alpha j - \alpha i\alpha i(rq - 1)$, with $q = 4.36$; $FS = 1.25$; $r = 2$ 29

Nomenclature

Abreviations

MEMS	Micro-Electro-Mechanical Systems
LOC	Lab-On-A-Chip
μ-TAS	Micro Total Analysis System
NMR	Nuclear Magnetic Resonance
DNA	Deoxyribonucleic Acid
SAR	Split-And-Recombine
PDMS	Poly(dimethylsiloxane)
CFD	Computational Fluid Dynamics
CAD	Computer Assisted Design
CDS	Central Difference Scheme
UDS	Upwind Differencing Scheme
HOT	Higher Order Terms
GCI	Grid Convergence Index

Greek Symbols

ρ	Density (Kg/m^3)
μ	Dynamic Viscosity (*Pa.s*)
α	Mixing Quality
σ	Standard Deviation
τ	Shear Stress (Pa)

Roman Symbols

Re	Reynolds Number
V	Cell Volume (m^3)
L	Channel Length (m)
D_h	Hydraulic Diameter of the outlet channel (m)

D	Molecular Diffusion (m^2/s)
H	Micromixer Height (m)
W	Channel Width (m)
A	Reference Area (m^2)
Q	Volumetric Flow Rate (m^3/s)
C	Concentration of a given fluid in a different one
t	Reference time (s)
u	Reference velocity (m/s)
Pe	Peclet Number
AR	Aspect Ratio of a T-Shaped Micromixer
I_s	Segregation Intensity
c	Mass fraction
N	Number of cells
m	Mass of a given fluid (Kg)
$\vec{n}$	Direction normal to the main flow
S	Mass-Distributed External Force (N)
g	Acceleration of gravity (m/s^2)
w	West side of a computational cell
e	East side of a computational cell
s	South side of a computational cell
n	North side of a computational cell
l	Lower side of a computational cell
h	Higher side of a computational cell
r	Grid Refinement Ratio
E	*Order of Grid Convergence*
q	Local order of convergence for three consecutive refinements
I_{KE}	Total kinetic energy rate transported at both inlets (W)

Subscripts

h	hydraulic
av	average
diff	diffusion
ia	inlet, side a
ib	inlet, side b
o	outlet
mix	mixing
c,máx	maximum concentration field
fluid i	refers to fuid I (fluid 1 or fluid 2)
exact solution	Value calculated by a Richardson Extrapolation as an estimate for the analytical

Chapter 1- Introduction

1.1 Motivation

Miniaturization is a subject that has had the attention of mankind since the XIII century, with the invention of the first clock. Later, in the XVII century, the microscope invention [1] allowed for the amplification of small-scaled objects images giving birth to the microscale observation. But it was only in the 80's of the 20th century that the microtechnology development attained a mature state with the advent of the MEMS (Micro-Electro-Mechanical Systems). Devices such as microvalves, micropumps, microfilters, micro-separators and micromixers are at the origin of a branch of fluid mechanics called microfluidics. This field of investigation is defined as the study of simple or complex, single or multi-phase flows in micro-systems [2]. Microfluidics is considered an emerging scientific field due to developments that allowed for the establishment of new protocols of manufacture and utilization, and because of the physical phenomena involved, which may be different from the ones at macroscopic scale [3]. The much smaller scale of such microdevices implies a much higher surface–to-volume ratio, *i.e.* the surface forces can no longer be overlooked.

In the 90's of the previous century, research carried out by Manz et al. [4] gave rise to applied devices with designations such as "lab-on-a-chip (LOC)" and "micro total analysis system (μ-TAS)". These devices have led to significant improvements on chemical, biological and biomedical experiments, with a remarkable reduction of waste, energy consumption and costs.

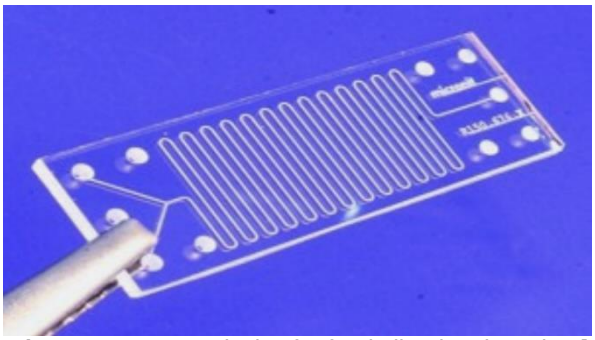

Figure 1. 1 *A LOC device for food allergies detection [5]*

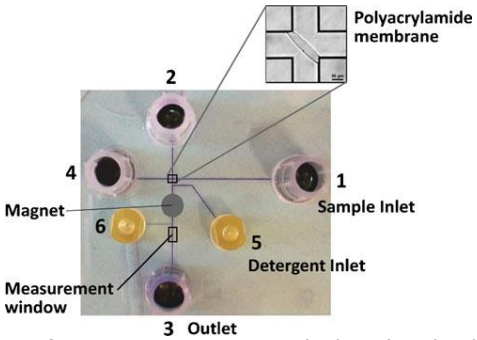

Figure 1. 2 *A LOC device for food allergies detection [5]*

The high portability is also a great advantage introduced by the LOC and μ-TAS devices [1,7] (figures 1.1 and 1.2).

The flows associated to such devices occur at very low Reynolds numbers (sometimes creeping flows[1]), so fluid mixing is one of the major challenges due to the high mixing lengths and times required [8,9].

1.2 State-of-the-art

Further development of LOC and μ-TAS devices is required, viewing improved and more efficient ways of mixing fluid flows at low Reynolds numbers, so that the required times and lengths are acceptable within the scale of the devices.

In the present section, the basics about internal flows and mixing will be presented, followed by a description of the current type of used micromixers. Then, special attention will be payed to T-shaped micromixers as the flow characterization within these devices constitutes the main concern of the present work. The final section of this chapter addresses the parameters that influence the performance of micromixers.

1.2.1 Internal Flows

Internal flows are generally classified as laminar, transition or turbulent, depending on the Reynolds number $Re = \frac{\rho U L}{\mu}$, ρ being the fluid density, U a characteristic velocity, L a characteristic length, and μ the dynamic viscosity of the fluid. The Reynolds number represents a ratio between inertial and viscous forces [10]. At low Reynolds numbers, the viscous forces are dominant and any perturbation is swiftly damped, and the flows have a deterministic nature. It is the so called Laminar Regime[11]. Fluid elements are organized as layers or lamellae and mass transport occurs mainly along the flow direction.

At Re≈2000-4000, the flow is in the laminar-turbulent transition regime, characterized by an increase of the inertial forces in such a way that any perturbation is advected to the whole field before being damped by the viscous forces. As Re continues to increase this behaviour becomes more conspicuous, leading to the disruption of the previous organized flow structure [10,11].

For higher Re the flow becomes fully turbulent. This regime is characterized by a chaotic behaviour and a strongly three-dimensional velocity field, thus allowing for mass, momentum and energy transport in all directions [10,11].

[1] It should be mentioned that a creeping or Stokes flow is a particular case of laminar flows with Re<<1.

For a circular cross-section, the internal diameter is usually considered the characteristic length in the calculation of Re. As the micromixers tested in the present work have a rectangular cross-section, a hydraulic diameter $D_h = \frac{2HW}{H+W}$ is defined instead, with H and W being the height and width of the channel, respectively.

In the present work, where the flow inside T-micromixers the Reynolds number is based on the hydraulic diameter of the mixing channel as characteristic length, and the average velocity V_{av} at the cross section, as characteristic velocity. From the definition of volume flow rate $Q = AV_{av} = HWV_{av}$, the equation for the Reynolds number used to characterize the flow inside T-micromixers becomes $Re_{D_h} = \frac{2Q\rho}{(H+W)\mu}$.

1.2.2. Fluid Mixing

When the mixing of the flows between two different miscible fluids occurs, the gradient of concentration of one of the fluids (or species) in the other reduces its intensity continuously until they reach equilibrium of concentration. This phenomenon can be mathematically described by the convection-diffusion equation [12,13]:

$$\frac{\partial C}{\partial t} + \nabla.(\vec{u}C) = -\nabla.(-D\nabla C) \tag{1.1}$$

with C being the concentration, t the time, $\vec{v}$ the velocity vector and D the molecular diffusion coefficient.

On the right-hand side of equation (1.1) the term $-\nabla.(-D\nabla C)$ represents the molecular diffusive transport, equal to minus the divergence of the molecular diffusive flux (Fick's law), whereas on the left-hand side the term $\nabla.(\vec{u}C)$ stands for the advection transport, equal to the divergence of the advective flux. Molecular diffusion smooths the species concentration gradients by molecule interactions while advection is related to the macroscopic transport of a property by the velocity field. The more intense and three-dimensional the velocity field is the better is the mixing.

To check the relative importance of diffusion and advection for a species concentration, the Péclet number is defined as follows [5]:

$$Pe = \frac{UL}{D} \tag{1.2}$$

with V being a characteristic velocity, L a characteristic length and D the molecular diffusion coefficient. A high value of Pe means that advection prevails, whereas diffusion is predominant for a low Pe [7,12].

1.2.3. Mixing Inside Microchannels

In microfluidic applications the characteristic lengths and the typical average velocities are of the order of 100μm and 0.1 to 1m/s respectively. As a result, typical Reynolds numbers for water flows range from 10 to 100 (for a kinematic viscosity of water equal to $10^{-6}m^2s^{-1}$ at 20ºC), which means that the flow is laminar [8,12,14].

Therefore, for a purely diffusive process the characteristic mixing time is [1]:

$$t_{diff} \sim \frac{l_{diff}^2}{D} \tag{1.3}$$

where l_{diff} is the diffusion length. Table 1.1 shows typical values of t_{diff} for some aqueous solutions.

Aqueous solution	**Diffusion Coefficient (m^2/s)**	$t_{diff}(s)$
Small ions in water	2×10^{-9}	5
Sugar molecules in water	5×10^{-10}	20
Enzimes and proteins in a micro-reactor	1×10^{-11}	1000

Table 1. 1 *Typical mixing times for mixing processes with a characteristic length of 100μm [15,16]*

The characteristic mixing time in the third case (enzimes and proteins in a micro-reactor) is 1000*s*, which shows the need to improve the mixing, all the more so because the mixture of enzymes and proteins in a micro-reactor is a typical application of LOC and μ-TAS devices.

1.2.4. Micromixers

Most authors [8,17-19] classify micromixers either by the type of application or by the use of external energy sources that promote mixing. The most widespread applications are: chemical, which include chemical synthesis, polymerization and extraction; biological, in DNA analysis, biological screening enzyme arrays and protein folding; detection/analysis of chemical or biochemical content combined with Nuclear Magnetic Resonance (NMR), Fourier Transform Infrared (FTIR) or Raman spectroscopies [5]. According to the use of external energy sources, the micromixers can be classified as active or passive, the latter operating without any kind of energy inputs [8,17-19].

In the present work, only passive micromixers will be analysed.

1.2.4.1 Active Micromixers

Active micromixers are devices where the mixing quality is improved by using external energy sources, which introduce vorticity in the laminar flow, thereby enhancing molecular diffusion [8,10,11,14]. A more accurate classification is shown in figure 1.3, according to the type of energy source used.

The attention given to this type of micromixers lies in the fact that they are considerably more efficient than the passive ones, thus reducing the characteristic mixing times and lengths. On the other hand, these systems are more complex, expensive and their application is more cumbersome since the external energy source must be coupled with the device itself [14].

1.2.4.2. Passive Micromixers

As explained before, passive micromixers are characterized by a mixing enhancement obtained from the geometrical configuration of the channels, the only external energy source present being the pumps that drive the flows into the micromixer. These devices can be categorized according to their purpose and geometry. As a general rule, the geometry should maximize the contact area between the fluids, in order to increase the diffusive transport. It should also promote local disruption of the deterministic structure of the laminar flow so that the advective transport is strengthened [7,8]. Among the micromixers that aim to maximize the diffusive

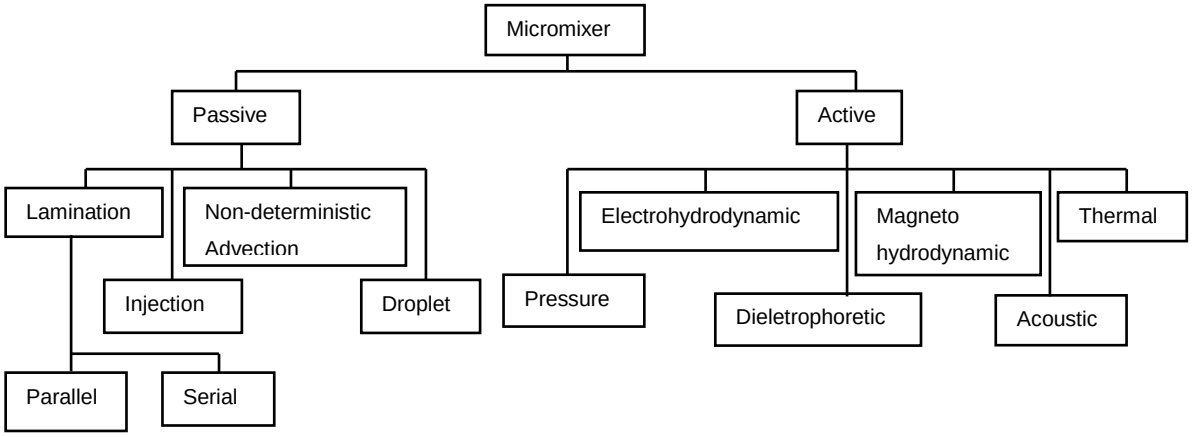

Figure 1. 3 *Classification of different types of micromixers [20]*

transport, the most relevant are multi-lamination micromixers and split-and-recombine (SAR) [7,14,20].

Both multi-lamination and SAR (figures 1.4 and 1.5, respectively) generate thin liquid lamellae, typically in the range of only a few to several tens of micrometres width, guiding them into a chamber where mixing occurs. Splitting the inlet streams into several streams and recombining them subsequently increases the contact area and promotes diffusion [14]. A considerable development has already been achieved in the LOC device [17,14].

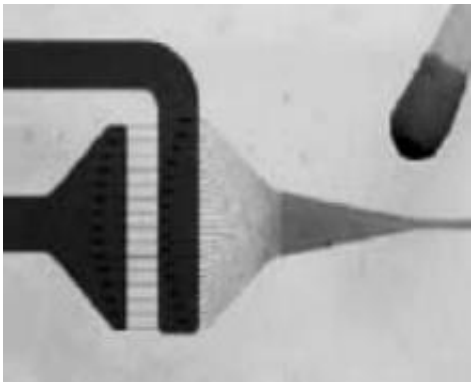

Figure 1. 5 *A multi-lamination micromixer [14]*

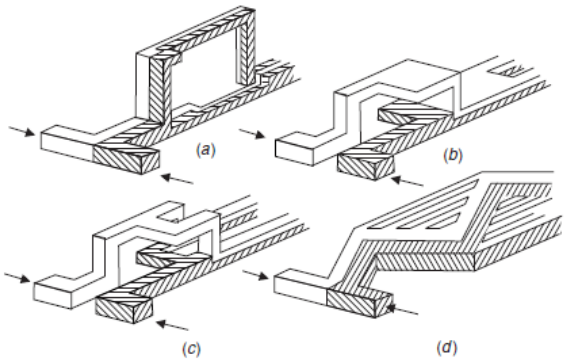

Figure 1. 4 *SAR micromixers. (a) Join-split-join, (b) split-join, (c) split-split-join, (d) multiple intersecting [20]*

Regarding the micromixers designed to promote advection, there are different geometrical solutions that increase it by promoting the appearance of non-deterministic flow structures. This phenomenon consists of the generation of three-dimensional flow structures, like vortices, with cross-flow velocity components that twist and curl the fluids interface, thus promoting a larger area of contact between the fluids [7].

The main geometrical solutions for non-deterministic advection are the following:

- The T-micromixers (figure 1.6) - among all the micromixers described in the present work, this has the simplest geometry. Two fluids, coming from different inlets, meet in the same mixing channel. Beyond a critical Reynolds number the interface between both fluids begins to twist and curl and is eventually disrupted, causing advective mixing related to the centrifugal forces [12,21].
- Zig zag micromixer (figure 1.7) - In this geometry, mixing is enhanced by laminar recirculation that induces secondary flow cells at the corners. Likewise, the disruption of the interface occurs beyond a critical Reynolds number, bellow which mixing is only due to molecular diffusion [7].
- Micromixers with obstacles, grooves and slots (figure 1.8) - In these geometries, three dimensional effects are induced by the insertion of obstacles along the walls of the microchannel, or inside the microchannel itself. The presence of obstacles alters the flow direction by making it more sinuous, thereby increasing the available mixing length. This solution has a low efficiency at low Reynolds numbers (typically bellow 100). Since obstacles increase friction losses, the pumping power to drive the fluids inside the micromixer also increases.

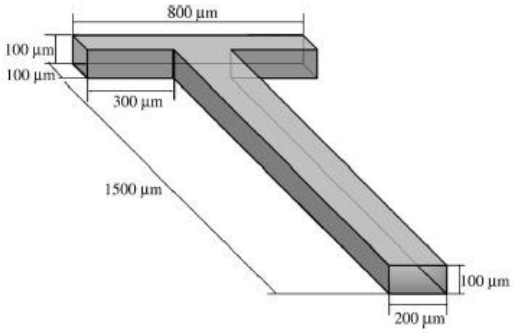

Figure 1. 7 *A T-shaped micromixer [17]*

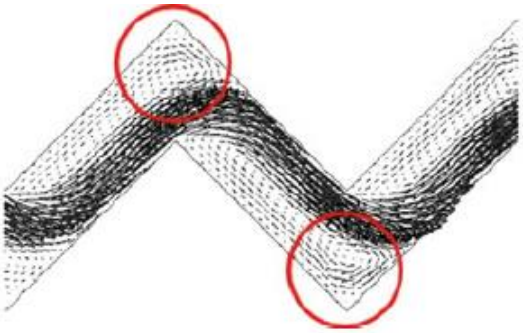

Figure 1. 6 *A zig-zag micromixer [7]*

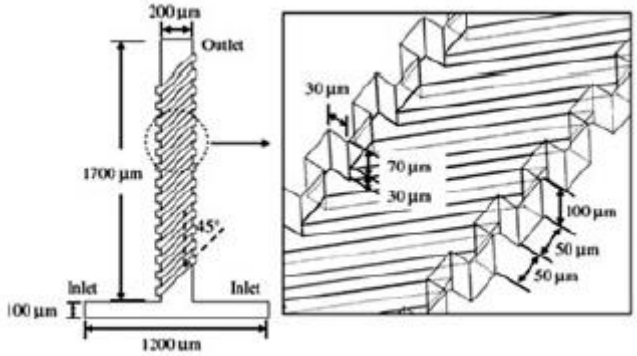

Figure 1. 8 *A connected-groove micromixer [7]*

The geometry that stands out from all those described above is the T-micromixer. Its simple design allows for cheap and fast production methods. In addition, having only two inlets and one outlet makes the T-micromixer easy to integrate into µ-TAS systems [22-25,9]. Moreover, compared to other solutions, friction losses along the walls are minimized which saves pumping power [23]. For these reasons T-micromixers were the choice of mixing microdevices made in the present work.

1.2.5 T-Micromixers

The T-micromixers, as schematized in figure 1.9, have two converging input channels of widths W_{ia} and W_{ib}, and a mixing (or outlet) channel of width W_o, where the mixing process takes place. The height H is constant throughout the geometry. The notation used to express the dimensions of a symmetrical micromixer is as follows: $W_i \times W_o \times H$, with the dimensions in µm [26-29].

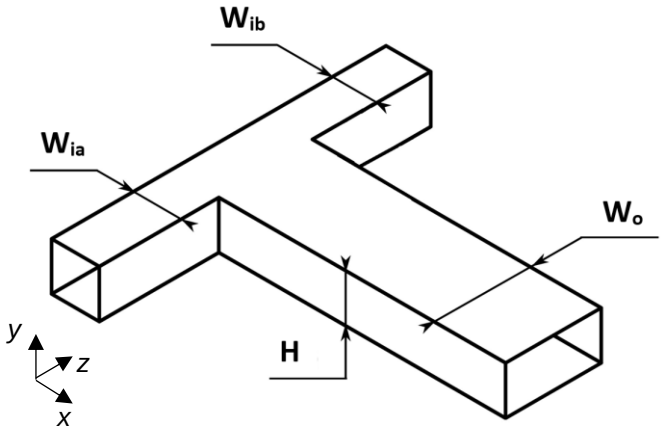

Figure 1. 9 *Representation of a T-micromixer of dimensions* $W_i \times W_o \times H$

The micromixer channels can also be defined according to their aspect ratio AR:

$$AR_{ia} = \frac{W_{ia}}{H} \tag{1.4.a}$$

$$AR_{ib} = \frac{W_{ib}}{H} \tag{1.4.b}$$

$$AR_o = \frac{W_o}{H} \tag{1.5}$$

1.2.5.1 Flow Regimes

Experimental and numerical studies have shown six different flow regimes. They can be either steady or transient and both have a strong dependence on the Reynolds number [39]. They are defined as follows:

- **Steady**
  - **Stratified Regime -** This regime exists for Re < 50 and is characterized by the fact that both fluid streams flow side by side in the mixing channel – see fig. 1.10.a. The cross-flow mass transfer is negligible [29]. The only mixing mechanism present is molecular diffusion.
  - **Vortex Regime -** For Re > 50 the vortex regime sets in and secondary flows arise due to centrifugal forces. Usually, a double vortex pair is observed, but the plane of symmetry perpendicular to the inlet channels is preserved. These secondary flow patterns cause a slight increase in the mixing quality [29].
  - **Engulfment Regime -** Transition to the engulfment regime occurs at Re≈150-240. This flow regime is characterized by the development of fine lamellae leading to a significant decrease in diffusion lengths. Rapid mixing is driven by secondary flows like vortices, as well as by boundary layer separation at the corners of the inlet channels [29].

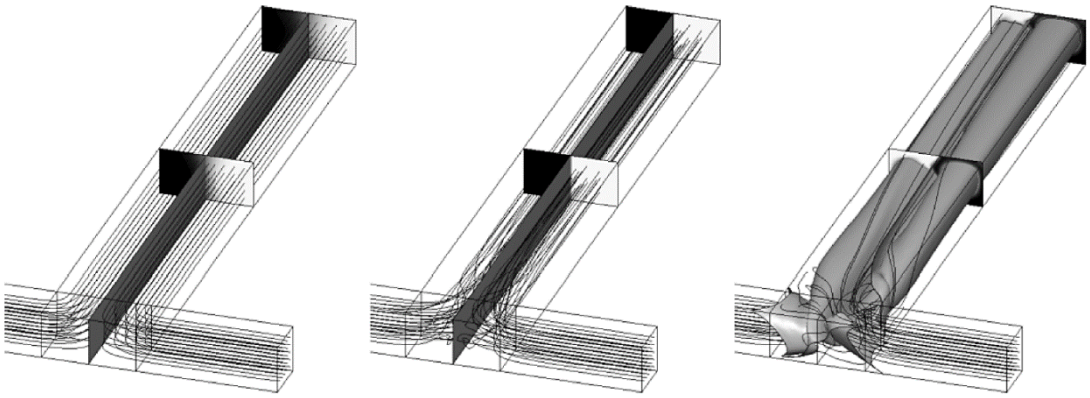

Figure 1. 10 *Schematic based on numerical results of the three steady flow regimes. a) stratified regime for Re=0.1, b) vortex regime for Re=130 and c) engulfment regime for Re=200*

- **Transient**
  - **Periodic Pulsating Flow (Figure 1.11) -** At around Re=300, the flow starts to exhibit transient characteristics. Periodically, the pair of vortices visible in the engulfment regime drifts towards the walls, eventually breaking down [12] and dissipating.
  - **Quasi-Periodic Pulsating Flow (Figure 1.12)-** For 400<Re<500 the flow recovers the symmetry present at a lower Re. The interface that separates both fluids oscillates horizontally and a pair of vortices containing fluid from the opposite side appear at each side. The rotation of these vortices oscillates between the clockwise and counter-clockwise direction. This behaviour can be parallelized to Kelvin-Helmholtz instabilities, particularly visible when the fluids interface is subjected to shear stress gradients due to their different densities or viscosities [12].
  - **Chaotic Pulsating Flow -** For higher Re the symmetry breaks down and the flow exhibits a chaotic[2] behaviour at the T-junction. Downstream, the flow becomes segregated again [12].

It should be noted that in the asymmetrical regimes advective transport exists only at the T-junction. Further downstream, in the mixing channel, the flow becomes laminar and molecular diffusion prevails again. In the symmetrical regimes, diffusion is the most important mixing mechanism in the entire channel.

[2] The term “chaotic” here, retrieved from the literature, does not contain any turbulence connotation, but refers to the non-deterministic character of the secondary flows

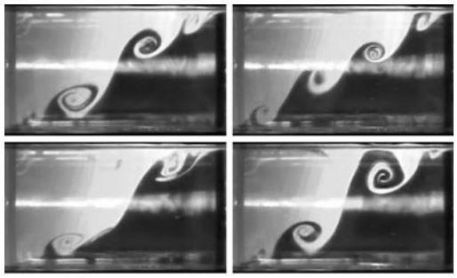

Figure 1. 12 *Periodic pulsating flow at Re=290 [30]*

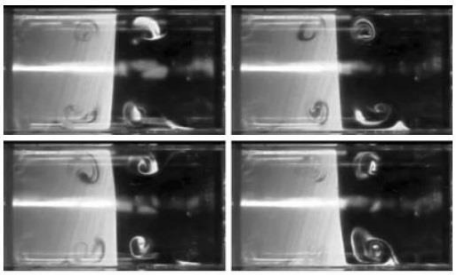

Figure 1. 11 *Quasi-Periodic Pulsating flow regime at Re=390 [30]*

1.2.6. Mixing Quality

To evaluate the performance of a micromixer, the definition of a parameter that quantifies the mixing quality achieved in such a device is required.

The most commonly used parameter takes into consideration the amplitude of the variations in concentration during the mixing process. This parameter is the mixing quality α_{mix}, suggested by Danckwerts, and is defined as [29,30,32,34],

$$\alpha_{mix} = 1 - \sqrt{I_s} = 1 - \frac{\sigma_c}{\sigma_{c,max}} \tag{1.6}$$

with I_s being the segregation intensity, σ_c the standard deviation of the concentration field, and $\sigma_{c,max}$ the maximum standard deviation of the concentration field. The value of α_{mix} varies between 0 and 1, with $\alpha_{mix} = 0$ corresponding to a system completely segregated and $\alpha_{mix} = 1$ to a homogeneous mixing. In the present case, as complete mixing is mathematically represented by mass fraction of a reference fluid equal to 0.5, and the maximum possible deviation from this value equals 0.5, Equation (1.6) can be rewritten in the following discrete form:

$$\alpha_{mix} = 1 - \frac{\sqrt{\sum_{i=1}^{N}(c_i - 0.5)^2}}{0.5\sqrt{N}} \tag{1.7}$$

where *N* represents the number of points with known concentration (in the present thesis this is the number of computational cells) considered in the calculation of α_{mix} and c_i is the mass fraction (concentration) of fluid i, which can be defined in a binary mixture as:

$$c_i = \frac{m_{fluidi}}{m_{fluid1} + m_{fluid2}}; i = 1,2 \tag{1.8}$$

where m_{fluid1} and m_{fluid2} stand for the mass of each fluid in a given computational cell. According to equation (1.8) $c_1 = 1$ in a cell where only fluid 1 is present. Otherwise, if in that cell there is only fluid 2, then $c_1 = 0$. A homogeneous mixing corresponds to $c_i = 0{,}5$. In the present thesis, water ($T = 293K$, $\rho = 998.16\ Kg/m^3$ and $D = 4.07 \times 10^{-8}\ m^2/s$) flows through both inlets, but fluid1 was labelled "water" and fluid2 was labelled "bromothymol". With this definition *c* represents the concentration of "bromothymol" in "water" in each cell.

This work introduces a new approach to evaluate the effects of the micromixers asymmetry on the mixing quality (the parameter α_{mix}). In fact, the usually used independent variable (the Reynolds number at the outlet channel) to classify the mixing quality (α_{mix}) [1,2,23,23,29] is certainly indifferent to the asymmetric conditions, *i.e.* one may have exactly the same Reynolds number value for an infinite number of combinations of different inlet flow rates. In the search for a parameter capable to account simultaneously for the increase of the Reynolds number (that is essential to understand the flow regimes above-described), and for the asymmetry of the device and/or inlet conditions, the choice was to use the transported kinetic energy rate at both inlets. Being a quantity transported by the fluid elements, this parameter is calculated from equation (1.9), where ρ is the fluid density, $\vec{v}$ is the velocity vector (with a magnitude of v) and $\vec{n}$ is the normal to the surface element *dA* that refers to both inlet channel cross-section areas *SC*.

$$I_{KE} = \int_{SC} \frac{\rho u^2}{2} (\vec{\boldsymbol{u}} \cdot \vec{\boldsymbol{n}}) dA \tag{1.9}$$

For the case of a flow in the direction normal to a cell face one has:

$$\frac{\rho u_z^3}{2} \Delta x \Delta y \tag{1.10}$$

1.2.7. Effect of Inlet Parameters on the Performance of T-Micromixers

1.2.7.1. Aspect Ratio

In the process of designing micromixers, the aspect ratio must be carefully controlled as this may have a significant impact on its performance.

A reasonable value must be assigned to the mixing channel aspect ratio AR_o, otherwise a too high or too low value will contribute to the flow stratification [34], downgrading the performance of the micromixer.

A mixing channel with an aspect ratio greater than the sum of the aspect ratios of the two inlets, $AR_o > AR_{ia} + AR_{ib}$, decelerates the flow at the T-junction, due to an increase of the cross-

sectional area. This allows for a better mixing of the fluids, increasing the time available for diffusion and decreasing the critical Reynolds number for the regime transition [33,35].

On the contrary, the use of a mixing channel such that $AR_o < AR_{ia} + AR_{ib}$, accelerates the flow at the T-junction and promotes segregation, increasing the critical Reynolds number for the transition to the engulfment regime [33,35].

In the present thesis, AR_o will be fixed at a value of around 2 as well as AR_{ia} that will have a fixed value of around 1. In turn, AR_{ib} will vary between 1.5 and 2, to understand how much the mixing quality can be improved by imposing geometric asymmetry to the inlets.

1.2.7.2. Asymmetries Between the Inlet Channels

A previous numerical work has addressed the subject of micromixers performance dependence on the viscosity and mass flow rate [36].

In the case of fluids with different viscosities, the mixing quality can improve as much as 50%. In the numerical simulations performed by the mentioned authors [36], one fluid had a viscosity that was twice the viscosity of the other. Observations have shown that the least viscous fluid was able to penetrate the other one near the upper and lower walls of the micromixer, thereby increasing the contact area and the mixing quality.

In a different work [19], the authors focused on mass flow rate asymmetry by using fluids with the same viscosity and imposing different flow rates at each inlet channel, ensuring that the experiments were in a range of Reynolds numbers based in the inlet hydraulic diameter between 125 to 350 and that the flow rate ratios (measured by the inlet flows Reynolds ratio), Re_{ia}/Re_{ib} have values of of 1.24, 1.65 and 2.45. It must be noted that flow rates ratio and Reynolds numbers ratio are equivalent only if the viscosity and density of the fluids entering both inlets is the same, which, as mentioned before, is the case. Once again the observations have shown that flow rate asymmetry favours the mixing quality. Another conclusion drawn by the authors referred to the greater impact of the inlet mass flow rates asymmetry on mixing than that of the asymmetry in the fluids viscosities.

1.2.7.3. Geometrical Asymmetries of the Inlet Channels

Recent research shows that using inlet channels with different geometries can improve significantly the performance of the T-micromixers [1,2,12].

Two experimental research works, in particular, constituted the starting point for the present thesis, using T-shaped micromixers aligned vertically and horizontally, but with different widths for the inlet channels. To conduct these experiments, different micromixers were

manufactured by soft lithography with poly(dimethylsiloxane) (PDMS) [22,23]. A flow of water was imposed at one inlet, and equal flow rate of a very diluted solution of bromothymol was imposed at the other. The experiments covered Re (based on the hydraulic diameter of the mixing channel) numbers from 50 to 310. Observations have shown five different flow regimes that are described below.

In Regime I (figure 1.13 a), at Re between 57 and 76, the flow is completely segregated, *i.e.* the inlet streams do not interfere with each other and a well-defined interface between both fluids is clearly visible. Molecular diffusion is the only mass transfer mechanism in this case [23].

At Re between 95 and 133, regime II occurs being characterized by the appearance of a residual advective mixing. The line defining the interface close to the T-junction deviates from the

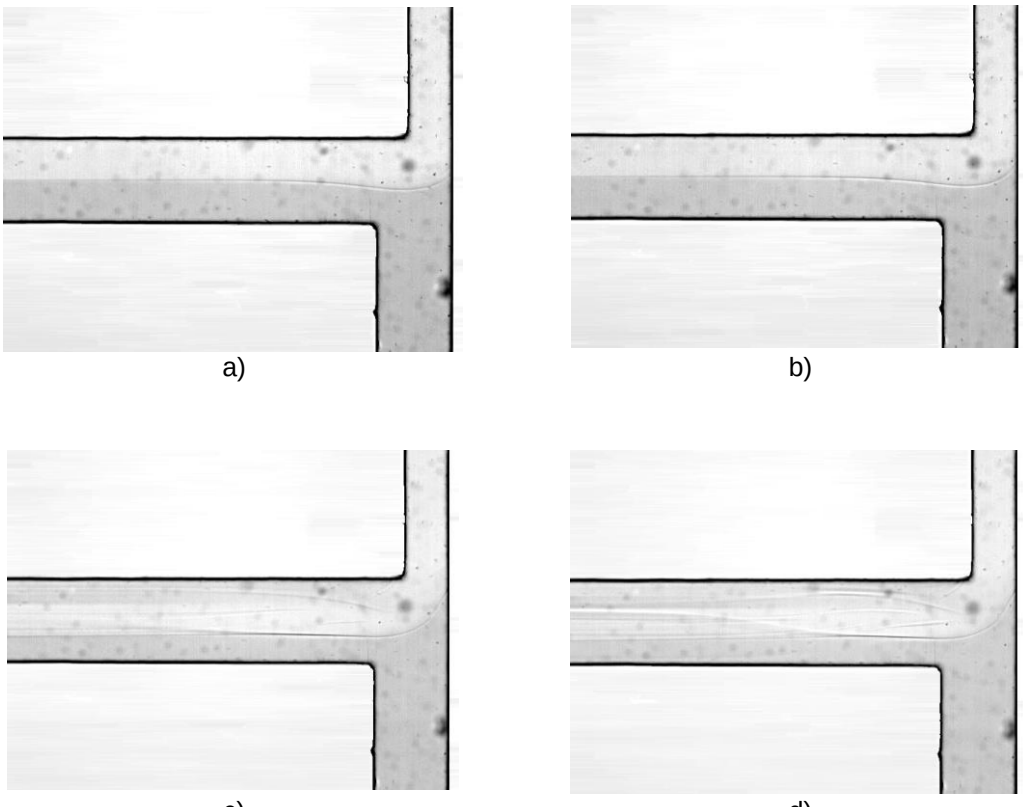

Figure 1. 13 *Flow visualization of a) regime I (Re_o=50), b) regime III (Re_o=100), c) regime IV (Re_o=222), d) regime V(Re_o=289) [23]*

horizontal symmetry axis, which means that the bromothymol solution, entering into the system through the wider inlet, is able to penetrate the water side. As a result, advection begins to play a pale role in the mixing process [23].

Regime III (figure 1.13 b) occurs for Re between 143 and 172. In this regime there is some bromothymol appearing close to the channel side wall in the water side, due to a local disruption of the interface separating both fluids [23].

Regime IV (figure 1.13 c), occurring for Re between 229 and 267, is characterized by the complete disruption of the interface that separates both fluids, which greatly enhances the mixing quality [23] as advection is now playing an important role.

Regime V (figure 1.13 d)), for Re above 267, is characterized by the generation of multiple vortices inside the mixing channel. The similarities to the symmetrical micromixer engulfment regime are clear. In addition, the flow also shows alternating layers of water and bromothymol solution superimposed, advection being the most important mechanism of mass transport [23].

The outcome of this research shows that increasing the level of asymmetry between the two inlets of the micromixer promotes the mixing quality. The critical Reynolds number for transition to regimes where advection plays a major role decreases, allowing for a faster and more efficient mixing, even at lower Reynolds numbers.

1.3 Objectives and Main Contributions of this thesis

Among the challenges existent in microfluidics, the ability to develop a device capable of promoting homogeneous mixing between fluids is currently one of great interest.

The T-micromixers stand out as an interesting solution due to its simple geometry, easiness of manufacture and low production costs. As described before, previous works [*1,2,12,19,22,23,36*] show promising results when asymmetrical inlet conditions are applied. Despite the fact that in the literature there is extensive work characterizing the flow inside symmetrical micromixers, there is no detailed characterization of the flow inside these devices when geometric asymmetry is applied. In fact, only global parameters are assessed in experimental works due to the experimental technique limitations [17,19,22,23,29,30,34,36].

As previous experimental works showed very promising results for geometrical asymmetries, but without characterizing the flows in detail due to the inherent limitations of the used techniques, the present thesis covers this gap of the knowledge by using numerical simulations (CFD – computational fluid dynamics) of the flows in such devices. Such kind of tool allows to get three-dimensional analysis of the flows inside T-micromixers and identify the physical mechanisms at stake. This makes possible the understanding of the influence of the asymmetry between inlets on the performance of the micromixers, and also how the increase of the Reynolds number induce the formation, or dissipation, of physical flow structures that define the five different flow regimes identified [22,23].

Five different geometries were modelled using CAD 3D Software Solidworks 2017. Three asymmetrical ones with different widths of the inlet channels, and two symmetrical ones, in which

one had smoothed corners in the mixing zone to characterize how geometric imperfections influence the mixing inside the micromixer. Then, using the Flow Simulation tool available in the above-mentioned software, twelve numerical simulations were performed per geometry, with Re_{D_h} varying from 25 to 295.

The numerical results were then exported as concentration plots in a section of the mixing channel, together with numerical values of concentration in the same section to perform the calculation of α_{mix},velocity to perform the calculation of $I_{KE}$and three dimensional views of the flow to allow for the identification of the physical structures involved.

1.4 Thesis Structure

The present work is organized in four chapters. In the first chapter, the reader is presented with the context of the work, the state-of-the-art, and the fundamental concepts that serve as basis for the work developed. In the second chapter the numerical techniques implemented in the commercial software are presented and explained. Chapter three is where the results obtained are presented and discussed. Finally, Chapter four serves as a wrap-up for the work developed and discussed previously, bringing conclusions and showing how this work brings innovation relatively to the literature. Also, this chapter presents recommendations for future work.

Chapter 2- Numerical Modelling

All the results from the numerical simulations were obtained using the commercial software *Solidworks Flow Simulation 2017* [37]. This choice was made due to the availability of a license and the fact that its graphical interface is user-friendly.

2.1 The studied T-micromixer geometries

The problem studied herein refers to the use of CFD to characterize the laminar flows at different regimes inside T-micromixers, both with symmetrical and asymmetrical inlet channels. Figure 1.9 of the previous chapter shows a geometrical scheme of such micromixers and table 2.1 displays the dimensions of the simulated micromixers.

Channel	$W_{ia}(\mu m)$	$W_{ib}(\mu m)$	$W_0(\mu m)$	$\frac{W_{ia}}{W_{ib}}$	L_0(mm)	H (μm)	$D_{h0}(\mu m)$
S1	100.31	100.31	200.63	1.00	3.00	100.94	134.30
A1	104.88	154.69	203.44	0.68	3.00	99.38	133.53
A2	102.19	175.31	200.63	0.58	3.00	99.38	132.91
A3	106.81	200.63	200.63	0.53	3.00	100.94	134.30

Table 2. 1 *Geometrical characteristics of the micromixers modelled. S2 geometry is not present as it has the same dimensions as S1, apart from the smoothed corners at the mixing zone.*

2.2 Governing Equations

Solidworks Flow Simulation is capable of predicting laminar as well as turbulent flows, but as the vast majority of flows are turbulent, this commercial code was developed especially to simulate the latter [37]. The governing equations of such turbulent flows, are applicable for a purely laminar flow, by setting the parameters k (turbulent kinetic energy, usually calculated by solving its transport equation) and μ_t (turbulent viscosity) equal to 0, which is the case of the present work.

Despite the fact that the simulations performed in this thesis correspond to steady state situations, the commercial software also solve the transient flow that precede the solution wanted. For that reason, in equations presented at the present this section and the ones that follow the time-dependent terms are not neglected.

The continuity and Navier-Stokes equations solved in the present work can be written, in Cartesian coordinates, as follows:

$$\frac{\partial \rho}{\partial t} + \frac{\partial}{\partial x_i}(\rho u_i) = 0 \tag{2.1}$$

$$\frac{\partial(\rho u_i)}{\partial t} + \frac{\partial}{\partial x_j}\left(\rho u_i u_j\right) = -\frac{\partial p}{\partial x_i} + \frac{\partial \tau_{ij}}{\partial x_j} + S_i \quad (2.2)$$

where x_i is the spatial i-direction, u_i is the fluid velocity component in the i-direction and ρ is the fluid density. The term S_i is a mass-distributed external force per unit volume and gathers three different contributions (i.e. $S_i = S_i^{Porous} + S_i^{Gravity} + S_i^{Noninertial}$) from: i) a porous media resistance (S_i^{Porous}) – nil in the present case, ii) a volumetric force due to gravity ($S_i^{gravity} = \rho g_i$, where g_i is the gravitational acceleration component along the i-direction) - nil in the present case and, iii) non-inertial effects if the coordinate system is accelerating ($S_i^{Noninertial}$) – nill in the present case . Moreover, τ_{ij} is the viscous shear stress tensor, defined as:

$$\tau_{ij} = \mu\left(\frac{\partial u_i}{\partial x_j} + \frac{\partial u_j}{\partial x_i} - \frac{2}{3}\delta_{ij}\frac{\partial u_k}{\partial x_k}\right) \quad (2.3)$$

In addition to the previous equations, *Flow Simulation* also solves the advection-diffusion equation for mass transfer in fluid mixtures, which runs for the specific m-component as:

$$\frac{\partial(\rho c_m)}{\partial t} + \frac{\partial}{\partial x_i}(\rho u_i c_m) = \frac{\partial}{\partial x_i}\left(D_{mn}\frac{\partial c_n}{\partial x_i}\right) + S_m \quad (2.4)$$

$$\sum_m c_m = 1 \quad (2.5)$$

Where D_{mn} is the molecular mass diffusivity tensor and S_m is the rate of production or consumption of the m-component, nill in the present case. Applying the Fick's diffusion law, the diffusivity tensor is:

$$D_{mn} = D\delta_{nm} \quad (2.6)$$

where D is a molecular diffusivity.

2.3 Numerical Technique

To solve accurately fluid simulation problems, *Solidworks Flow Simulation* makes available a great variety of techniques and algorithms based on the *Finite Volume Method*. This method entails by subdividing the computational domain into a fixed number of control volumes, which constitute the computational mesh [37]. The computational domain includes both the entire region of study, *i.e.* the microchannel volume and the empty space corresponding to the outside of the microchannel. This empty space represents a waste of computational effort (mainly memory) that must be minimized. Figure 2.1 shows the geometry and computational domain for the micromixer A3, used to check the accuracy of *Solidworks Flow Simulation* and the grid

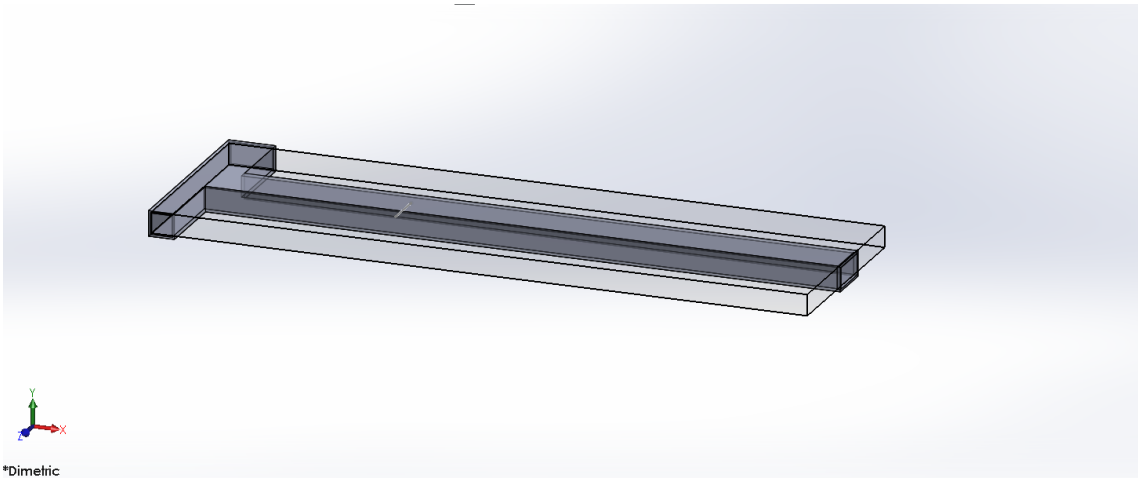

Figure 2. 1 *Representation of the most asymmetric micromixer A3 and the computational domain used. The latter is the volume enclosed by the parallelepiped represented exterior space does not participate in the numerical simulation.*

independence of the numerical solutions.

2.3.1 The Computational Mesh

Since *Solidworks Flow Simulation* uses Cartesian coordinates, the yielded cells have a parallelepipedic shape. Grid generation involves several steps. It starts with the imposition of a certain number of cells N_x, N_y and N_z, along the three orthogonal directions, which yields a basic mesh with a total amount of $N_T = N_x \times N_y \times N_z$ finite volumes, including fluid cells, solid cells and empty space. The second step involves the refinement of the first-built basic mesh, since some of the cells intersect the solid walls. This is done with a numerical tool of *Solidworks Flow Simulation* known as *Cartesian Cut Cells Approach*. With this technique, whenever there is an intersection with a solid-fluid interface, the mesh cells are subdivided into smaller polyhedrons in order to preserve the solid-fluid interface as close to the reality as the modeller wishes (Figure 2.2) [37].

The next step involves defining the desired degree of refinement. *Solidworks Flow*

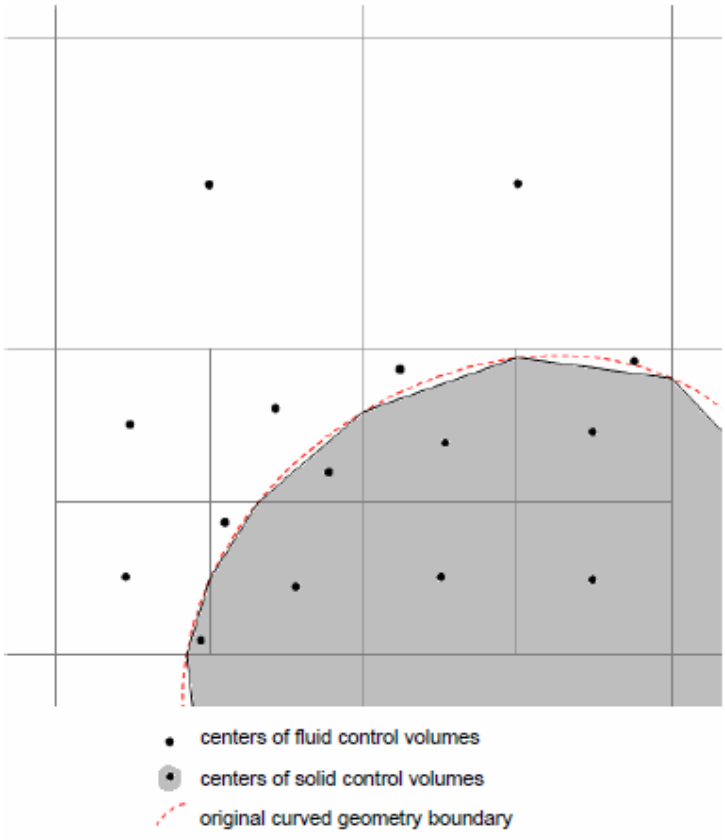

Figure 2. 2 *Example of a mesh near the solid-fluid interface [17]*

Simulation defines refinement levels, the basic mesh being *level 0*, and *level 1* resulting from the division of each basic mesh cell into 8 cells. Therefore, if the refinement is done uniformly, the level 1 mesh has $8N_T$ cells and the *level* 9, considered the maximum level of refinement, has $8^9 N_T$

cells. The refinement can be done in different regions of the computational domain and according to different criteria. In the present work, the refinement was applied only in regions where there is fluid and is especially important whenever large gradients, of any property, are expected in the flow.

2.3.2 Spatial Discretization

As described above, the method used to discretize the governing differential equations constitutes the *Cell Centred Finite Volume Method*. The aim is to obtain algebraic equations by integrating the differential equations in a control volume, which is a mesh cell surrounded by 6 adjacent cells whose centres are located East (E), West (W), North (N), South (S), High (H) and Low (L) of the current cell (Figure 2.3). All variables are computed at the centre P of each cell. Applying the divergence theorem, the volume integral of the divergence of the convective and diffusive fluxes is equal to the surface integral of these fluxes. Taking, as an example, equation (2.4<), the finite volume formulation yields [38] equation (2.7), where $S^* = \bar{S}V_P = S_U + S_P y_p$ and $A_w, A_e, A_s, A_n, A_l, A_h$ are the areas of the cell faces and V_p is the cell volume.

$$\frac{(\overline{\rho c_P^{t+1}} - \overline{\rho c_P^{t}})V_p}{\Delta t} = \left(\rho u c_P - D\frac{\partial c_P}{\partial x}\right)_w A_w - \left(\rho u c_P - D\frac{\partial c_P}{\partial x}\right)_e A_e + \left(\rho v c_P - D\frac{\partial c}{\partial y}\right)_s A_s - \left(\rho v c_P - D\frac{\partial c_P}{\partial y}\right)_n A_n + \left(\rho w c_P - D\frac{\partial c_P}{\partial z}\right)_l A_l - \left(\rho w c_P - D\frac{\partial c_P}{\partial z}\right)_h A_h + S^* \quad (2.7)$$

The overbars on the left hand side term, stand for the average value in the cell and S^* is a space-time averaged source term. As this method is solved in its fully implicit form, the parameters

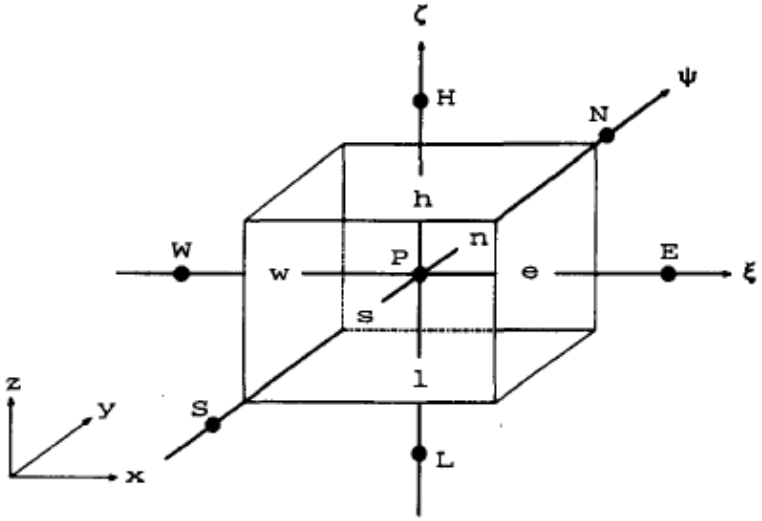

Figure 2. 3 *A typical cell. Capital letters represent neighbouring cells and small letters the cell faces [20].*

present in the right hand side are evaluated in the instant “t+1” Likewise equation (2.4), which represents a mass balance in an infinitesimal control volume, equation (2.7) represents the same balance but in a finite control volume [15,37-39].

The diffusive and convective fluxes are computed at the centre of each face. For the former, a *Central Difference Scheme* (CDS) is used, in which a linear profile is assumed for the variable *y*, between two adjacent cells. For instance, the diffusive flux between P and E becomes [38]:

$$\left(D\frac{\partial c}{\partial x}\right)_e A_e = \lambda_e(c_E - c_P) \tag{2.8}$$

with,

$$\lambda_e = \frac{DA_e}{x_E - x_P} \tag{2.9}$$

Combining equations (2.8) and (2.9) yields:

$$\left(\frac{\partial c}{\partial x}\right)_e = \frac{c_E - c_P}{x_E - x_P} \tag{2.10}$$

As far as convective terms are concerned, the scheme used is the *Upwind Differencing Scheme* (UDS). It merely consists in setting the value y_e equal to its upstream value [38,39]:

$$c_e = \begin{cases} c_P \ , \ (\vec{u}\cdot\vec{n})_e > 0 \\ c_E \ , \ (\vec{u}\cdot\vec{n})_e < 0 \end{cases} \tag{2.11}$$

The UDS has the advantage of not producing oscillatory solutions that other schemes may generate, however it may lead to *numerical diffusion*.

It should be noted that the methods presented so far for equation (2.4), are also valid for the discretization of the other equations solved by *Solidworks Flow Simulation.*

2.3.3 Temporal Discretization

The continuity and convection-diffusion equations are discretized with an implicit scheme. This means that for any variable ϕ, an equation such as:

$$\frac{\partial \phi}{\partial t} = F(\phi) \tag{2.12}$$

becomes, after discretization:

$$\frac{\phi^{t+1} - \phi^t}{\Delta t} = F(\phi^{t+1}) \tag{2.13}$$

where n stands for the current time step and n+1 for the next time step $t+\Delta t$.

The implicit discretization method is unconditionally stable, i.e. it always produces bounded solutions, since the errors inherent to the discretization do not amplify [39].

An implicit discretization of the momentum equations implies an iterative procedure. In the *Solidworks Flow Simulation* software this is done with the SIMPLER algorithm [40].

2.4 The Studied Case

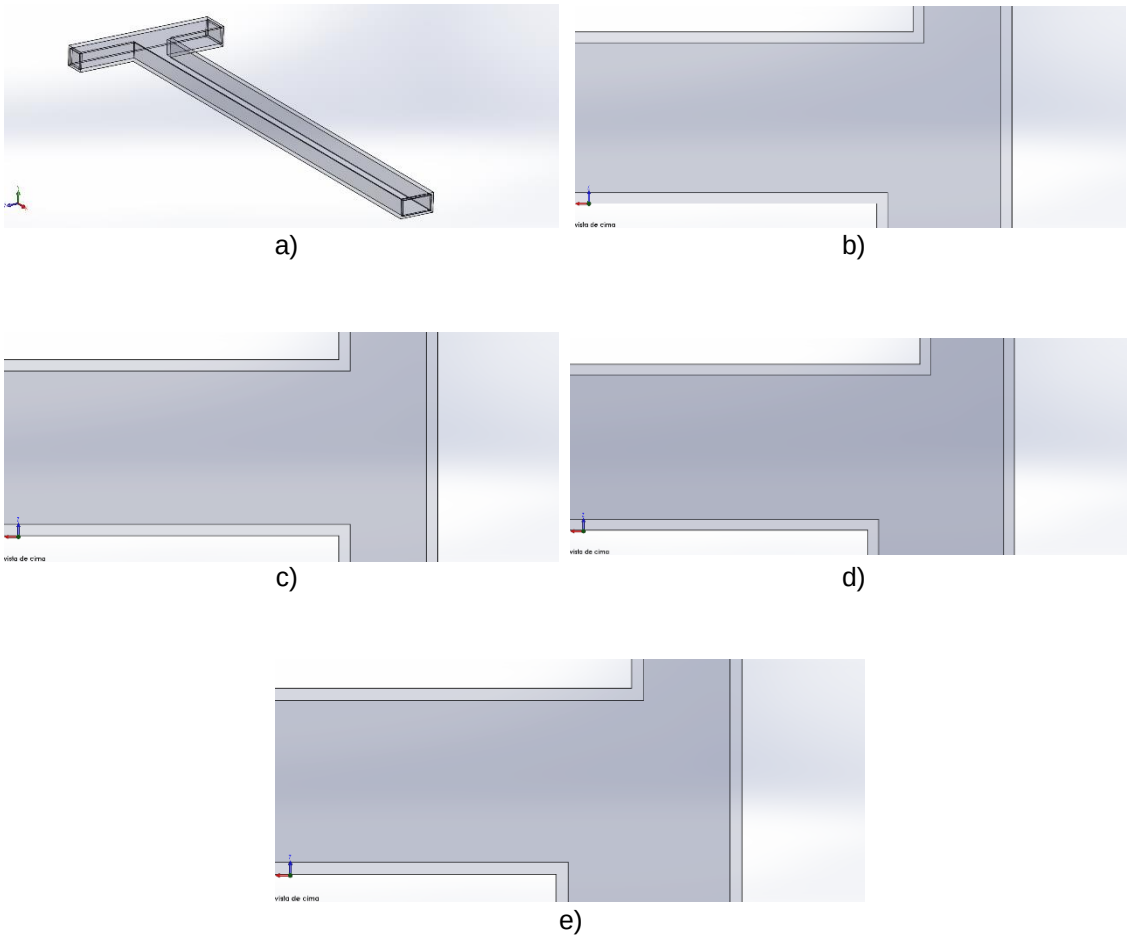

Figure 2. 4 *CAD models of the micromixers. a) General 3D view of the micromixer A1 b), c), d), e) top views of longitudinal cross-sections of micromixers A1, S1, A2 and A3*

2.4.1 Geometries modelled

To compare the numerical solutions with the corresponding experimental results obtained in previous research works [2], four CAD models with the same dimensions as the experimental were generated, as shown in figure 2.4[3].

It should be noted that the computational domain is the same for all geometries, avoiding several sensitivity analysis regarding grid dependence of the numerical solutions. If the numerical results, for the simulation which exhibits the most complex flow patterns, do not depend on the grid size and time step, the same behaviour is expected for the other cases. The most complex case corresponds to the most asymmetrical geometry, A3, at the highest Reynolds number.

2.4.2 The Computational Mesh

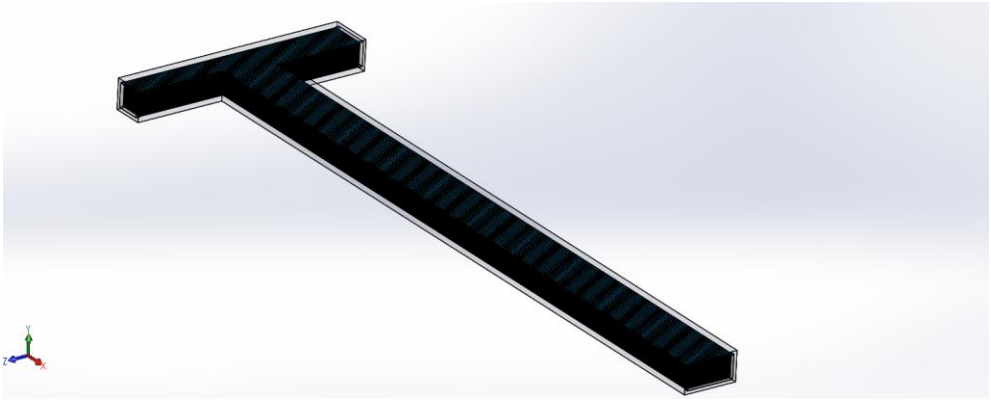

a)

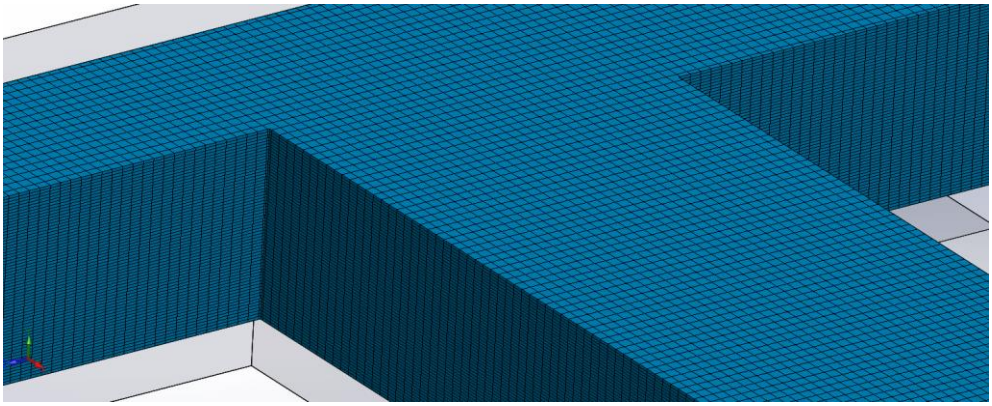

b)

Figure 2. 5 *Computational mesh. a) General view. b) A close-up view of the mixing zone of the A3 geometry*

[3] The correspondence between the micromixers designations in this work and those of the experimental work is: A1-B1, A2-B5, A3-B4, S1-B3 [2]

Using the software of grid generation and refinement, the mesh obtained for the A3 geometry is shown in Figures 2.5 a) and b).

According to the notation of *Solidworks Flow Simulation* it is a level 4, 30x4x10 mesh. It means that the basic mesh has dimensions 30x4x10 and is refined 4 times (2^4 in each direction), so the actual mesh to perform the numerical simulation has dimensions 480x64x160. If the entire computational domain were refined, this would result in 4 915 200 cells, but since refinement applies only to the region where there is fluid, the total number of cells is 1 246 080. As mentioned previously, all the geometries have the same settings for grid generation, which implies that they have roughly the same number of fluid cells. Moreover, the computational mesh is uniform, i.e., the grid size is constant.

Theoretically, the mesh should be more refined where velocity (or other relevant variables) gradients are expected to be larger, saving computational time. However, preliminary results have shown that, in addition to boundary layers and the more obvious mixing zones at the entrance region (T-zone), large concentration gradients also occur across most of the mixing channel, forcing the need to have a sufficiently refined mesh throughout the entire computational domain. Another problem that arises is numerical diffusion. With *Solidworks Flow Simulation* the modeller has no choice between several schemes for the discretization of the convection term. Therefore, numerical diffusion can only be controlled choosing an appropriate value of the cell Peclet number, which measures the relative importance of convection and diffusion. Since for a low Peclet number diffusion prevails, the cell Peclet number should be kept as low as possible to avoid numerical diffusion. Of course this implies refining the mesh to maximum possible levels (computer-memory dependent) [38-40]. As Cartesian coordinates are being used, a coarse grid also exhibits the disadvantage of not being sometimes oriented with the flow, which is another major source of numerical diffusion. In the present case, the meshes generated have Peclet numbers as high as 14000, the lowest values being around 200. These are quite large numbers, so some numerical diffusion is expected in the present results.

2.4.3 Initial and Boundary Conditions

Since the solution method of the algebraic set of equations is iterative, an initial guess of the velocity field and mass fraction field is mandatory. Hence, the velocity was set equal to 0 in the whole computational domain and equal mass fraction in both inlets, *i.e.* a mass fraction of 0.5 for each of them.

With respect to the boundary conditions, a no-slip condition is imposed, as well as a condition of impermeability along the solid boundaries, *i.e.* tangential and normal velocity components are set to zero in these regions.

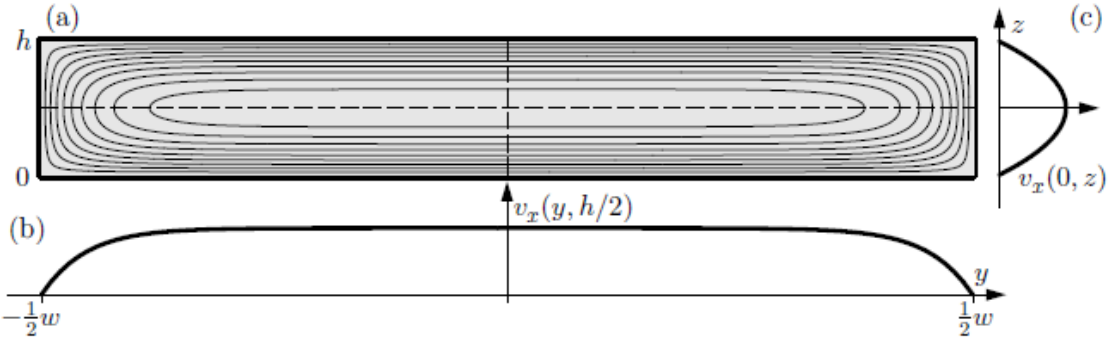

Figure 2. 6 *Representation of the velocity profile at both inlet streams for a Poiseuille flow inside a rectangular cross-section channel [16]*

At the outlet, atmospheric pressure is prescribed, and at both inlets the volume flow rate is imposed. *Solidworks Flow Simulation* assumes at the inlets a Poiseuille-type flow in rectangular cross-section channels (fully developed in the *x*-direction), *i.e.* it assumes the following two-dimensional velocity profile at both inlets (Figure 2.6, [16]):

$$u(x,y) = \frac{24Re_{hD}(h+w)\nu}{\pi^3 hw}\sum_{n,odd}^{\infty}\frac{1}{n^3}\left[1-\frac{\cosh\left(n\pi\frac{y}{h}\right)}{\cosh\left(n\pi\frac{w}{h}\right)}\right] sin\left(n\pi\frac{z}{h}\right)\left[1-\sum_{n,odd}^{\infty}\frac{192h}{n^5\pi^5 w}\tanh\left(n\pi\frac{w}{2h}\right)\right]^{-1} \quad (2.14)$$

2.4.4 Convergence criteria

From the various options of *Solidworks Flow Simulation* for the convergence criterion, the one that yielded the best results, with a minimum of computational effort, was the "Global Average" with $\delta = 5\%$, where $\delta = Min(\nabla_{curr}, \nabla_{av})$. Note that ∇_{curr} corresponds to the difference between the minimum and maximum values the control variable has along the calculation, whereas ∇_{av} is the difference between the maximum and minimum values of the average value of the control variable over the previous iterations. In the present case, the control variables considered to check convergence were the average values over the entire computational domain of the three components of velocity, total pressure, and mass flow rate. *Solidworks* assumes these variables as "Global". The value of 5% was obtained by trial and error, assuming first 50% and progressively decreasing this value until the results no longer depend on the convergence criterion.

2.4.5 Grid Convergence Study

A grid convergence study was performed to verify the spatial convergence of the numerical simulation. As the mesh is refined, the numerical values of a given variable tend asymptotically to the exact solution [41].

Since the cells do not have a cubic shape, the characteristic grid spacing considered was $h = \sqrt[3]{V_{cell}}$, with V_{cell} being the volume of a cell. For this test, the parameter used was α_{mix}, a global parameter of mixing quality inside the micromixer. Five simulations were performed. Table 2.2 shows the evolution of α_{mix} with h:

h (m)	6.20E-05	3.10E-05	1.55E-05	7.78E-06	3.91E-06
α	0.897	0.644	0.557	0.475	0.471
index for the mesh	5	4	3	2	1

Table 2. 2 *Evolution of α_{mix} with h (characteristic grid spacing parameter) for the numerical simulations performed*

Some control variables must be defined: the first one is called *grid refinement ratio*, which quantifies how much smaller the cells are, after successive refinements [41]. As after one refinement each cell is divided into 8 cells, the coarser grid has a characteristic grid spacing that is twice the finer one. This parameter is constant for all refinements and is equal to:

$$r = \frac{h_2}{h_1} \tag{2.15}$$

with h_1 being the characteristic grid spacing of the finest mesh. For the two most refined meshes, and according to table 2.2, $r = h_2/h_1 = (7.78 \times 10^{-6})/(3.91 \times 10^{-6}) = 1.99 \approx 2$.

The second control variable is called *order of grid convergence*. This parameter quantifies the difference between the numerical solution and the exact solution, defined as [41],

$$E = f(h) - f_{exact} = C \times h^p + H.O.T. \tag{2.16}$$

with C being a constant, h the grid spacing, p the order of convergence and *H.O.T.* standing for Higher Order Terms. A value of 2 for the order of convergence is generally acceptable.

The exact solution is estimated using a *Richardson Extrapolation*, which is defined (adapted for the present case and assuming an order of convergence of 2) as follows:

$$\alpha_{exact} \cong \alpha_1 + \frac{\alpha_1 - \alpha_2}{r^2 - 1} \tag{2.17}$$

In the previous equation, $\alpha_1$and $\alpha_2$are the mixing quality value for the two most refined meshes, respectively (see Table 2.2). Substituting values, equation (2.17) yields:

$$\alpha_{exact} \cong 0.471 + \frac{0.471 - 0.475}{2^2 - 1} = 0.470$$

Neglecting the higher-order terms (H.O.T.) in equation (2.16) and applying the logarithm, yields [41]:

$$\log(E) = \log(C) + p\,\log(h) \tag{2.18}$$

From equation (2.19), p corresponds the slope of the straight line $\log(E)$ as a function of $\log(h)$, E being defined from Equation 2.18 as:

$$E = \alpha_i - \alpha_{exact} \tag{2.19}$$

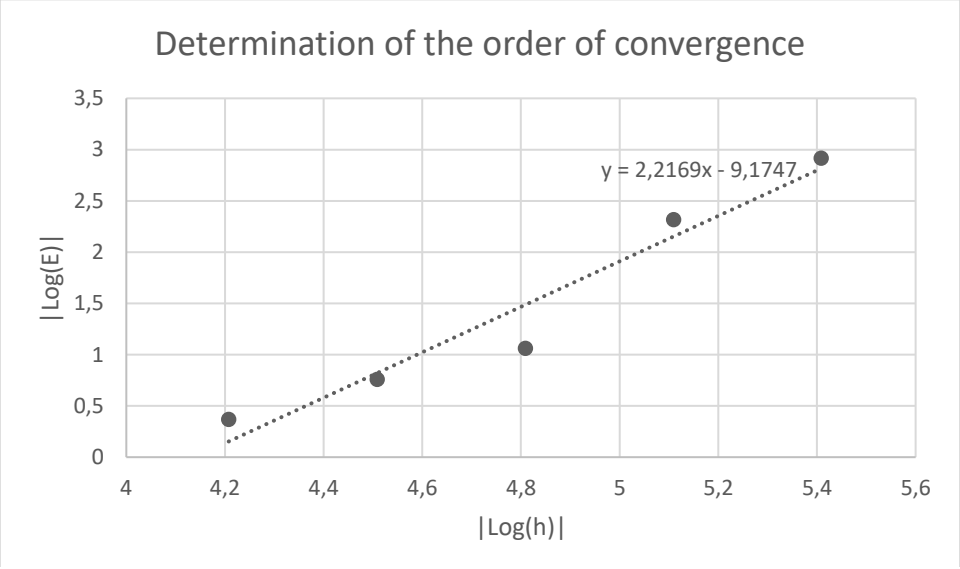

Figure 2. 7 *Plot of Log(E) versus Log(h). Modules have been taken because E and h are lower than one*

This straight line is plotted in figure 2.7.

The value estimated for p is equal 2.2, close to 2. Therefore, the numerical solution has a good rate of convergence.

The third control variable is the *Grid Convergence Index (GCI)*. This parameter represents a percentage of how much α_{mix} is expected to change if a further refinement of the mesh is performed. The GCI for a grid refinement (say, using grids 1 and 2) yielding results α_1 and α_2, respectively, is defined as [41]:

$$GCI_{12} = \frac{F_s\left|\frac{\alpha_2 - \alpha_1}{\alpha_1}\right|}{(r^q - 1)} \tag{2.20}$$

where F_s is a safety factor. A value $F_s = 3$ is recommended for the comparison of only two grids and $F_s = 1.25$ for more than two grids [41]. As the order of convergence was estimated with 3 grids, $F_s = 1.25$ will be considered. The subscripts of the variables (e.g. GCI_{12}, α_1 and α_2) point to the values of Table 2.2 used in the calculations.

Moreover, when consecutive solutions are already in the asymptotic range of convergence, the following relation is found[41]:

$$GCI_{23} = r^q GCI_{12} \tag{2.21}$$

where $GCI_{23} = F_s \left|\frac{\alpha_3 - \alpha_2}{\alpha_2}\right| / (r^q - 1)$, and the index 3 refers to the third grid, *i.e.* to the value of α correspondent to the third most refined solution – see Table 2.2.

The appropriate value of the local order of convergence q to be used in equations (2.20) and (2.21) can be estimated from the three most refined solutions. According to Roache [41], such q value is equal to:

$$q = \frac{\ln(\frac{\alpha_3 - \alpha_2}{\alpha_2 - \alpha_1})}{\ln r} \tag{2.22}$$

Substituting values yields:

$$q = \frac{\ln(\frac{0.557 - 0.475}{0.475 - 0.471})}{\ln 2} = 4.36$$

With such q value, GCI_{12} and GCI_{23} can now be calculated:

$$CGI_{12} = \frac{1.25 \left|\frac{0.475 - 0.471}{0.471}\right|}{(2^{4.36} - 1)} = 0.000543$$

$$CGI_{23} = \frac{1.25 \left|\frac{0.557 - 0.475}{0.475}\right|}{(2^{4.36} - 1)} = 0.011046$$

Substituting values in equation (2.21) yields:

$$GCI_{23} = r^q GCI_{12} <=> GCI_{23} = 2^{4.36} 0.000543 <=> GCI_{23} \cong 0.011$$

Table 2.3 represents the evolution of the GCI index from the coarsest to the finest meshes and also verifies the equality 2.21

Index	$GCI_{ij} = \frac{F_s \left\lvert \frac{\alpha_j - \alpha_i}{\alpha_i} \right\rvert}{(r^q - 1)}$	$GCI_{ij,ass} = r^q GCI_{i-1,j-1}$	$\left\lvert GCI_{ij} - GCI_{ij,ass} \right\rvert$
GCI_{45}	0.025183	0.20526	0.1800
GCI_{34}	0.010011	0.22686	0.2168
GCI_{23}	0.011066	0.01116	0.00004
GCI_{12}	0.000544	----	---

Table 2. 3 *Analysis of the* Grid Convergence Index *for the studied meshes* $GCI_{ij} = \frac{F_s \left\lvert \frac{\alpha_j - \alpha_i}{\alpha_i} \right\rvert}{(r^q - 1)}$, *with* $q = 4.36$; $FS = 1.25$; $r = 2$.

The value 0.00004 for $\left\lvert GCI_{23} - GCI_{23,ass} \right\rvert$ suggests that mesh 1 is already within the asymptotic range of the computed solution, so it is considered that grid convergence is achieved.

2.4.6 Data Post-Processing

The data obtained from the numerical simulations done for this thesis that were exported for image processing consisted of:

- velocity components in the entire flow domain for flow visualization using stream tubes and isovelocity surfaces (figure 2.8 a)).
- 1300 values of water mass fraction in the mixing channel, at a cross section located at 1057μm away from the common wall to both inlets, exported from *Solidworks*.
- water mass fraction in the middle plane of the micromixers (figure 2.8 b)), and in a plane 40 μm distant from the middle plane (figure 2.8 c));
- concentration in a cross section located at a distance from the common wall equal to 1057μm (figure 2.8 d));

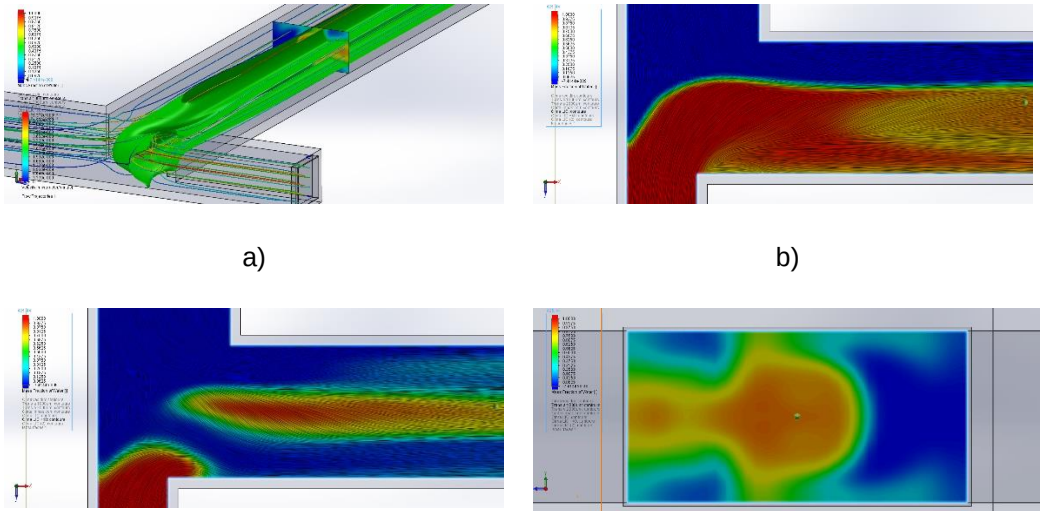

a) b)

c) d)

Figure 2. 8 *Example of exported images and plots exported from SolidWorks Flow Simulation. a) flow visualisation, b) water mass fraction in the middle plane of the micromixers, c) water mass fraction in a plane at 40 μm distant from the middle plane of the micromixers, d) concentration in a cross section located at a distance from the common wall equal to 1057μm.*

Chapter 3- Presentation and Discussion of Results

One of main goals of this chapter is the identification of the fundamental physical structures governing the flow inside asymmetrical T-shaped micromixers, particularly as far as mixing effects between streams are concerned, and the way they are affected by the increase of the flow rate and/or the geometry. To be more specific, three different degrees of asymmetry are going to be studied, namely 0.68, 0.58 and 0.53, as presented in table 2.1. The other main goal is the comparison for validation purposes of the numerical predictions with experimental results previously obtained by other authors [1,2], the numerical results constituting a complementary information that otherwise would not be possible to obtain.

The reference case is the symmetrical one, due to its greater geometrical simplicity and widespread use, exhibiting a number of flow regimes smaller than in the asymmetrical cases, but with an abrupt transition between the vortex and the engulfment regimes, which occurs for the larger Reynolds numbers[4]. Moreover, and to understand how geometrical imperfections inherent to the manufacture process of microchannels can influence the mixing quality inside the micromixer, a comparison will be made between a geometrical model with perfect 90º corners at the micromixer junction and a version with such corners smoothed out resembling those of the experimental work.

Next up the flow inside the assymetrical micromixers and its influence on the degree of mixing are discussed. The first topic covers the influence of increasing the Reynolds number (and higher velocities attained), followed by the study of the influence of different levels of assymetry on the performance of the device.

The parameter used to evaluate the performance is, as discussed before, the α_{mix}. This parameter has been widely used in the literature [1,2,12,17,21-23] since it is a very effective way to compare results from different authors. In the work presented in this thesis α_{mix} is evaluated through the use of equation 1.7 with 1300 points from a section of the mixing channel located at 1057μm away from the common wall of the two inlets. The variable used for the calculation of α_{mix} was the concentration of one of the streams in the other, as described in section 1.2.6. In the experimental work, the fluids used were distilled water and a very diluted aqueous solution of Bromothimol. The goal was to have both streams distinguished by their colour intensity, and still have similar physical properties.

As in the numerical simulations both streams are distinguishable even though the same fluid enters both inlets, water was set to enter in both. They are distinguished by setting the concentration equal do 1 at one of the inlets, and labeling the fluid entering as “Water”, and setting the concentration equal to 0 at the opposite inlet, and labeling the fluid entering as “Bromothymol”.

[4] It should be noted that the stratified regime is the one occurring for low Reynolds numbers.

To accomplish the goals established, four different micromixers were modelled –see table 2.1. One of them is, as referred above, the symmetrical case. As the name suggests, this geometry consists of two inlet channels that are geometrically identical, and an outlet or mixing channel. A stream of water and one of a dilute bromothymol solution enter each inlet (at equal flow rates), they meet halfway, and continue downstream the mixing channel, where mixing occurs. From an experimental point of view, it is very important to figure out a way to visualize the flow and discriminate elements of fluid coming from different inlets; so, the logical solution is the application of a marker (mostly rhodamine B or bromothymol [1,21-23,37,42,43]) to one of the streams to ensure the required contrast for flow visualization and make the evaluation of the mixing quality possible. As for the numerical predictions, both streams are distinguishable downstream by their colour in the concentration plots set in the commercial software. The colour gradient goes from red (water) to blue (bromothymol), and colours in between represent different levels of mixing of both. Stream tubes of both fluids have the same colour, but in this case with no gradient. A stream tube starting in the narrower inlet is coloured red and a stream tube that starts in the larger inlet is blue.

The three other geometries modelled are asymmetrical, exhibiting therefore differences in the width of the inlets – see table 2.1. Equal volume flow rates are imposed in both inlets, so different average velocities, and consequently kinetic energy and momentum transported by fluid elements, are expected to improve mixing quality.

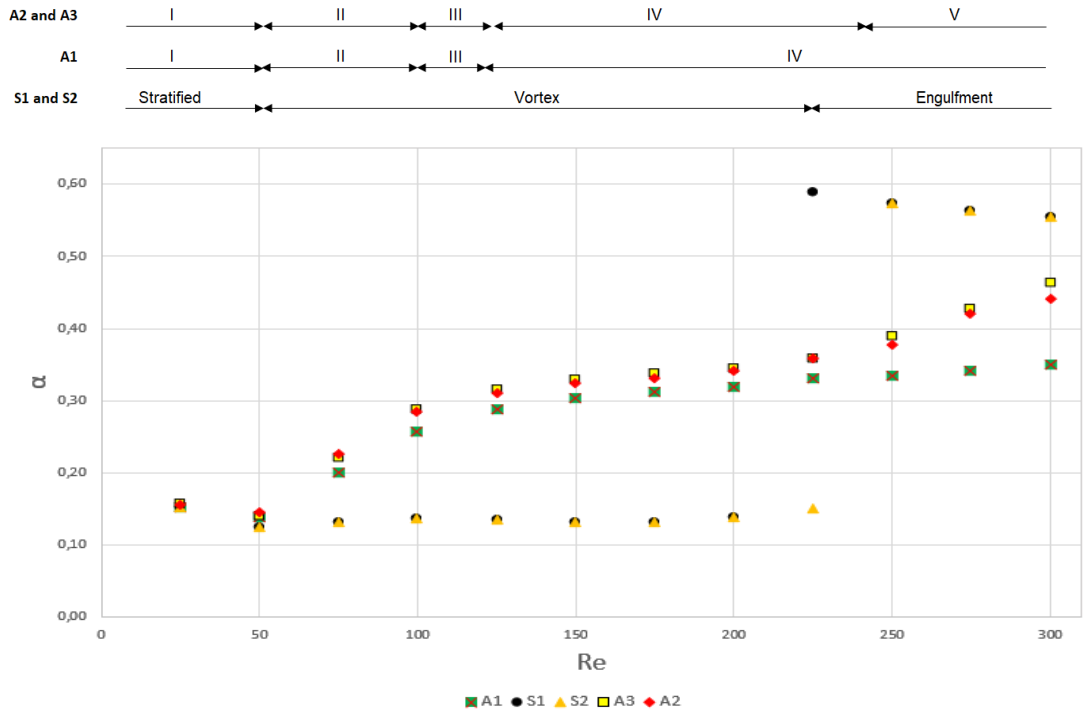

Figure 3. 1 *Mixing quality α_mix as a function of the Reynolds number (Re) for the mixers S1 (black circles), S2 (yellow triangles), A1 (green squares with red cross), A2 (red diamonds) and A3 (yellow squares with black lining). Above the plot there is also a representation of the flow regimes identified for the devices. Orange arrows correspond to the three regimes identified for symmetric micromixers, the green arrows stand for the regimes identified for A1, and blue arrows represent the micromixers A2 and A3.*

The results will be presented and discussed by appealing to different visualizations, such as 3D streamlines, plane streamlines, and coloured plots of specific planes, which will facilitate the identification of the physical phenomena at play.

The starting point for this discussion is Figure 3.1, which is a plot that represents the variation of the mixing quality parameter α_{mix}, with the Reynolds number (Re). Firstly, the symmetrical case is discussed, then the attention in turned into the asymmetrical micromixers by looking to the influence of Reynolds number increment, and finally a study on the influence of the degree of geometrical asymmetry on the performance of these devices is performed.

3.1 The symmetrical case

In figure 3.1 it is possible to clearly identify 3 flow regimes, similarly to other authors' results [12,17,21,34,35,42]

Up to Re ≈ 50 (Fig.3.2a and b) the so-called *Stratified Laminar* flow regime exists. It is characterised by a segregated flow with straight parallel streamlines in the mixing channel, with little, or no advection. Consequently, the only mixing mechanism acting is molecular diffusion. It can be observed in the figure 3.1 that for this regime the mixing quality is poor and drops with increasing Re. This behaviour is due to the fact that the increase of Re brings an increase of the velocity field and, consequently, the residence time of the fluid particles inside de mixing channel decreases. As explained before, being the residence time such an important parameter in molecular diffusion-driven processes, they have less time to mix [12,21], when the fluid particles travel faster.

From Re ≈ 50 onwards the three-dimensional effects together with the centrifugal force experienced by the fluids in the T-junction region become important, and the flow is in the so-called *Laminar Vortex* regime *(Fig.3.2c and d)*. This regime is characterized by the appearance for each incoming stream of two large and slow counter-rotating axial vortices (parallel to the axis of the mixing channel) in the T-junction region – see figure 3.2c and d. These four vortices form due to the deflection of both fluid streams caused by the centrifugal force induced by the walls presence, but downstream they are dissipated by the viscous forces and the streamlines end up straightening [42,44]. Another two small (with strong rotation) vortices form next to the wall common to both streams. The geometry of the micromixer implies that the momentum transported by both inlet fluid streams is cancelled, inducing the conversion of kinetic energy into pressure energy. This increase of pressure in the mixing zone creates a local adverse pressure gradient. In the *Laminar Vortex Regime*, the adverse pressure gradient is already so severe that flow separation occurs and one vortex for each side form in the recirculation zone. As Re increases the vortices present in the micromixer grow in intensity, but as the interface does not break up, the mixing quality remains unchanged. Molecular diffusion is the most important mixing mechanism. The growing intensity of the vortices can only make up for the decreasing residence time, and worse mixing that comes with it [42].

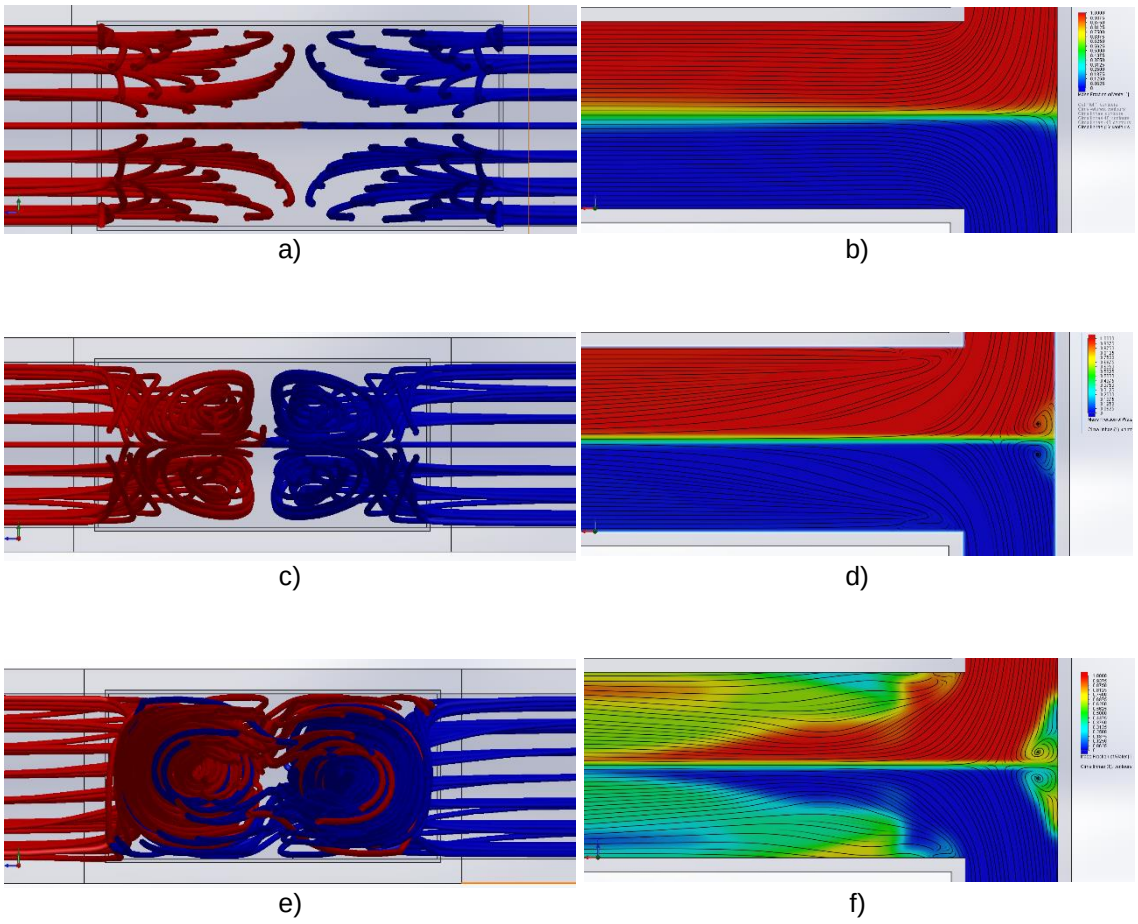

Figure 3. 2 *Images representative of the three identified regimes for the flow inside the micromixer S1. a) and b) are for Re=25 in the stratified laminar regime. c) and d) are for Re=150 in the laminar vortex regime. Finally, e) and f) show the results for Re=250 in the engulfment regime. The images a), c) and e) represent a front view of the mixing channel with 100 stream tubes, 50 for each fluid. Red tubes are water and the blue ones are bromothymol. The images b), d) and f) show a colour plot of the mass fraction of water in the middle plane between upper and bottom walls of the micromixer. They also show the streamlines in the same plane.*

At Re ≈ 225 (Fig.3.2e and f) the fluids interface breaks up, and the flow enters the *Engulfment Regime*. In this regime there are portions of each fluid stream going into the opposite side, *i.e.* penetrating into the other fluid flow. The pairs of vortices of the previous regime degenerate into two bigger vortices that promote the mixing of each fluid entering in one side with the other coming from the opposite side. Here, the stagnation point in the mixing zone and the two adjacent vortices also play their part in promoting the improvement of the mixing quality by advection. In Fig.3.3 it is also possible to confirm the absence of flow separation downstream the 90º corners, by the inexistence of flow recirculation. This phenomenon is likely to be associated to the conversion of kinetic energy into pressure energy in the mixing zone, due to momentum cancelation of both fluid streams. Consequently, the pressure gradient in the 90º degree corner becomes more favourable, and flow separation does not occur.

Downstream the mixing zone, the streamlines still straighten up, but with no interface separating both fluids. Instead, what can be observed is the existence of small lamellae (Fig.3.3a), resulting in shorter diffusion lengths, thus improving diffusion mechanisms [23]. Figure 3.3b also

shows another interesting mechanism. The two small vortices near the common wall develop at different locations, *i.e.* one of them can be seen in the upper region of the micromixer, whereas the other grows towards the bottom region (that is why in the image only one vortex is discernible). This structure plays an important role in the mixing process as it deflects the water flow towards the mixing channel. It is also interesting to note that most of the water flows to the bromothymol side by the upper region. On the other hand, most of the bromothymol flows to the water side by the bottom region of the micromixer. It is clear that advection is the mechanism playing the most important part in this regime with many flow structures developing, which reflects on the enormous increase in the mixing quality.

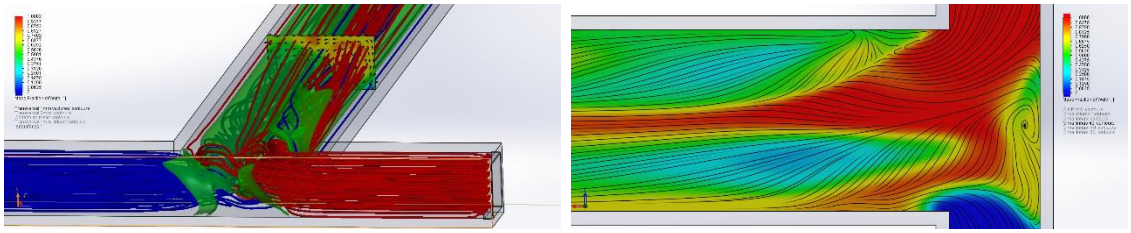

a) b)

Figure 3. 3 *Aditional representations of the flow inside micromixer S1 at Re=250. Image a) is a perspective that allows to get a general overview of the flow. It was made with 50 stream tubes for bromothymol and 50 for water. It was also introduced an isosurface for a mass fraction of water of 0.5. The aim was to get an estimate for the location of the interfaces water-bromothymol. It is possible to see a colour plot for the mass fraction of water for the cross-section where* α_{mix} *is being evaluated. Image b) shows a colour plot of the mass fraction of water in a plane that is 40μm of the midplane. This plot also shows streamlines for the flow in this plane.*

For this Reynolds numbers range, although advection is very important for the mixing quality, diffusion still plays a relevant role.

Increasing further the Reynolds number results in a slight decrease of the mixing quality α_{mix}, as it can be seen in Fig. 3.1. This is expected, since no new structures appear and the water/bromothymol interface is already disrupted. Hence, increasing the volume flow rate inside the micromixer results in shorter residence times and, therefore, in a lower molecular diffusion mixing capacity.

A final conclusion was drawn on how geometrical imperfections in the manufactured microchannels may influence the results. In Figure 3.1 a direct comparison between the results for microchannels S1 and S2 evidences that imposing a smoother corner in the mixing zone delays the flow transition to *Engulfment Regime*. The reason for this behaviour is most likely that

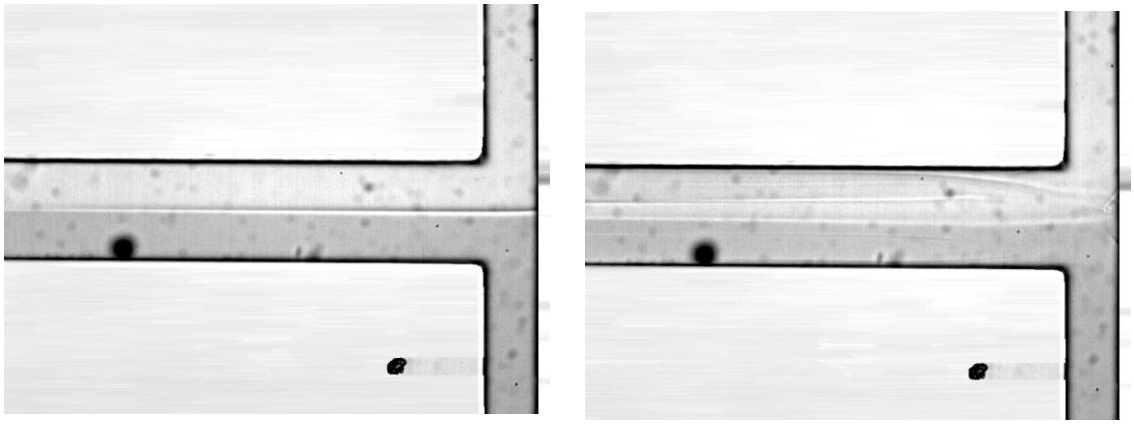

a) b)

Figure 3. 4 *Images for the flow inside a symmetrical micromixer similar to the one modelled (S1). a) and b) stand for Re=140 and Re=156, respectively [2].*

this way the intensity of the pair of vortices induced by the centrifugal forces induced on the fluid elements when going round the smoothed corner is lower compared to the ones induced when the corner is 90º sharp, thus delaying the rupture of the interface separating both fluids. As rupture occurs, micromixer S2 matches S1 in performance, just like in every other simulation before this near transition zone. Apart from this phenomenon, S2 exhibits the same physical structures as S1. One can therefore state that geometrical imperfections have a significant impact on flow transition. Other works from the literature [12,21,35] follow these same conclusions by claiming that transition is expected to occur between Re ≈ 120 to Re ≈ 300, depending on the geometry and flow conditions.

Comparison of Fig.3.4b and Fig.3.2f evidences that the similarities are clear, but with transition occurring at Re ≈ 156 for the experimental data whereas in the numerical simulation this occurs at Re ≈ 225. Also, the values calculated for the mixing quality α_{mix} are 0.14 and 0.23 for figure 3.4 a) and b) respectively. The value for the first case follows closely what was found for S1 in the numerical calculations. In the second case, the value is significantly different from the magnitude of the values calculated for α_{mix} in the present work. In the experimental work, there is geometrical imperfections that influence the performance of the micromixer. But also, α_{mix} was calculated from the photographs taken at the microdevices, using the microscope. These images were treated, and the contrast of the pixels evaluated to estimate α_{mix}. But this value is influenced by the focal plane of the microscope. The operator tried to focus the middle plane, but there is an uncertainty associated as there are no guarantees that the focal plane was indeed the middle plane of the micromixer, and the adjacent planes are likely to influence the picture. Another clear factor that may influence the calculation α_{mix} in the experimental work, and can be observed in

figure 3.4 is the presence of noise and inclusions in the acquired images. Although the subsequent treatment helps mitigate these effects, in cannot be completely eliminated.

Figs.3. 5a and b that exhibit other authors' [34] results also show similarities with the work presented herein, but some differences may arise due to geometrical differences, different boundary conditions and even different diffusion coefficients (artificially changing the diffusion is a common strategy carried out by many authors to keep characteristic Peclet numbers at moderate values avoiding the numerical diffusion of coarse meshes).

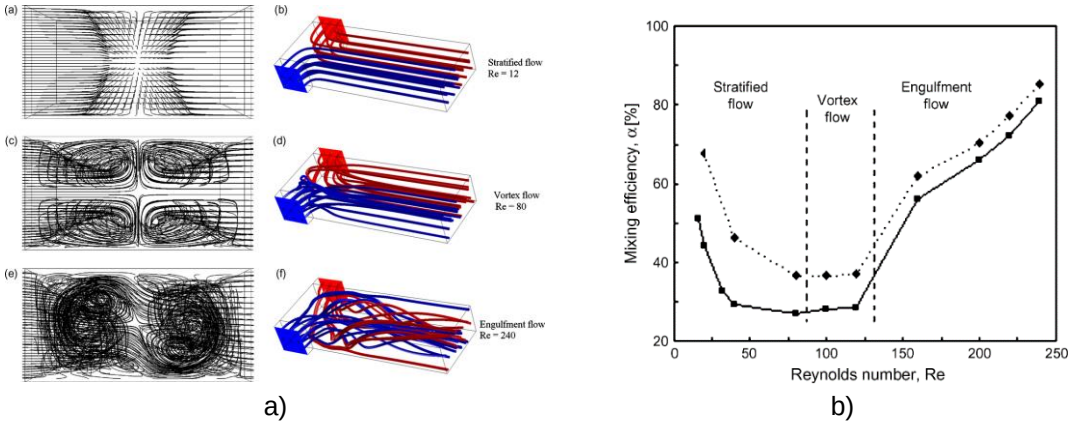

Figure 3. 5 *Similar work [34]. a) flow streamlines and tubes for Re=12, Re=80 and Re=240. b) α plot as a function of Re for two different values of diffusion coeficient (D=2×10^(-7) m^2/s for the squares and D=1×10^(-6) m^2/s for the diamonds)*

3.2 The Asymmetrical Micromixers

3.2.1 Effect of the Reynolds number and flow regimes

Looking at Figure 3.1 from a global point of view, it is clear that the increase of the Reynolds results in increasingly better mixing quality, with α_{mix} growing throughout the range of the simulations carried on. A first difference in comparison with the symmetrical micromixer is the inexistence of a sudden transition to the so-called *Engulfment Regime*. It is possible to identify up to five different flow regimes (that will be discussed in this section), and it is unquestionable the superior performance of the asymmetric micromixer in the Re range 75-225. However, the symmetrical micromixer yields a higher mixing quality than the asymmetrical one after the transition to the *Engulfment Regime*, with the value of α_{mix} decreasing for larger Re as discussed above. This parameter increases steadily for the asymmetrical micromixer, and at Re = 295 the performances of the symmetrical and asymmetrical micromixers are similar, with the first having α_{mix}=0,55 and the latter α_{mix}=0,45, but showing very distinct tendencies. The value for the symmetrical micromixer follows a slight decreasing trend, while for the asymmetrical ones show a consistent increase.

3.2.1.1 Regime I

At Reynolds numbers bellow 25 the flow inside asymmetrical micromixers is similar to the *Stratified Laminar* regime encountered for the symmetrical case. Figures 3.6a and b show both fluids entering the mixing channel with no advection at the outlet channel and the presence of a clear interface separating the streams. A slight perturbation in the interface in the mixing zone can be observed, which is caused by the larger momentum of the water fluid elements, being able to push the flow towards the bromothymol inlet channel. Downstream the mixing zone this interface becomes a high concentration gradient zone possessing a thickness that grows as the distance to the mixing zone increases (figure 3.6c). This is an evidence of the molecular diffusion mechanism at work in this regime. Molecular diffusion is, in fact, the only mixing mechanism present in this regime. Up until Re ≈ 25, α_{mix} decreases because the fluid particles residence time will be smaller with a larger velocity field, so they will have less time to mix.

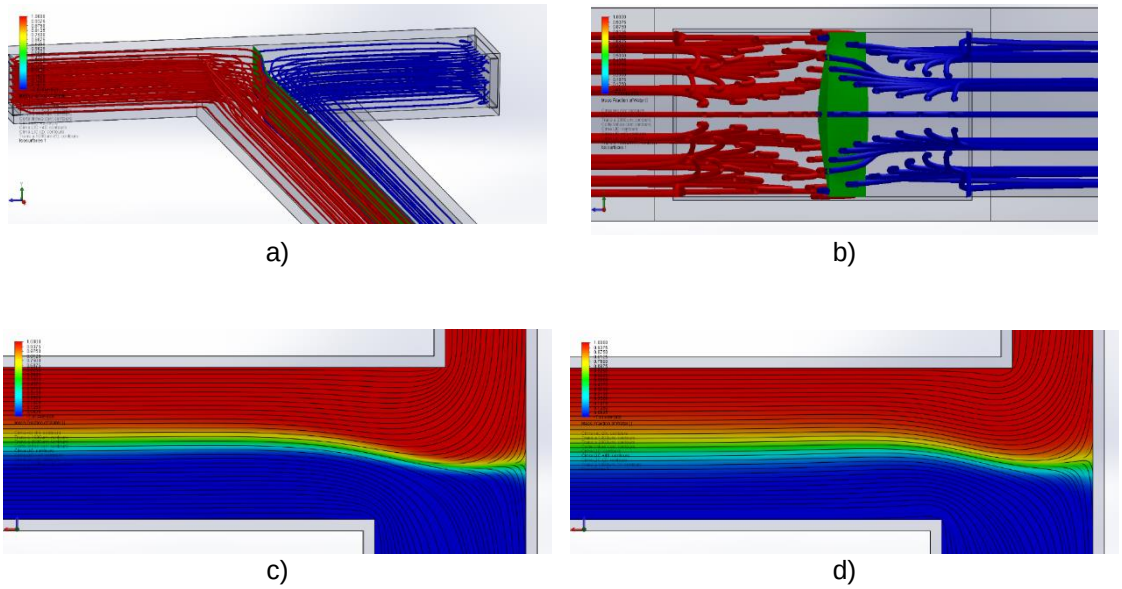

Figure 3. 6 *Representative images of the flow inside micromixer A3, the most asymmetrical, at Re = 25. a) Perspective view of the mixing zone, is constituted by 50 tubes of each fluid and an isosurface of mass fraction of water equal to 0.5. b) View inside the entire mixing channel, constituted similarly to a). c) Colour plot of the mass fraction of water in the middle plane between the upper and bottom walls of the micromixer, with streamlines. d) Same representation, but now in a plane that is 40μm above the middle one.*

3.2.1.2 Regime II

For Reynolds numbers above 50 it is possible to witness a shift in the above-described trend: the mixing quality starts to increase considerably. Although at the midplane the flow inside the micromixer exhibits similarities with those at lower Reynolds numbers (figure 3.7e), at the upper and lower planes there is bromothymol passing to the water side. The perturbation in the water-bromothymol interface is the major responsible for this phenomenon to occur. As explained before, this perturbation is caused by the water fluid elements that carry larger momentum than those of bromothymol.

But, in opposition to that occurring in the previous regime, for regime II the bromothymol fluid elements divert to the upper and lower planes of the micromixer. Additionally, the shape of the water-bromothymol interface in the mixing zone helps to direct bromothymol fluid particles to the mixing chamber. In the mixing zone, the interface is slightly shifted to the bromothymol side due to the higher kinetic rate and momentum transported by the water fluid elements. This fact also contribute for the diversion of bromothymol to the upper and lower planes of the micromixer. The combination of these facts results in an improved mixing process as it is possible to see in figure 3.7a and b. Bromothymol fluid elements that were diverted towards the planes above and below the middle one possess more momentum than water fluid elements already in this zone (it should be noted that near wall regions are characterized by lower velocities [10,11, 44]), allowing these

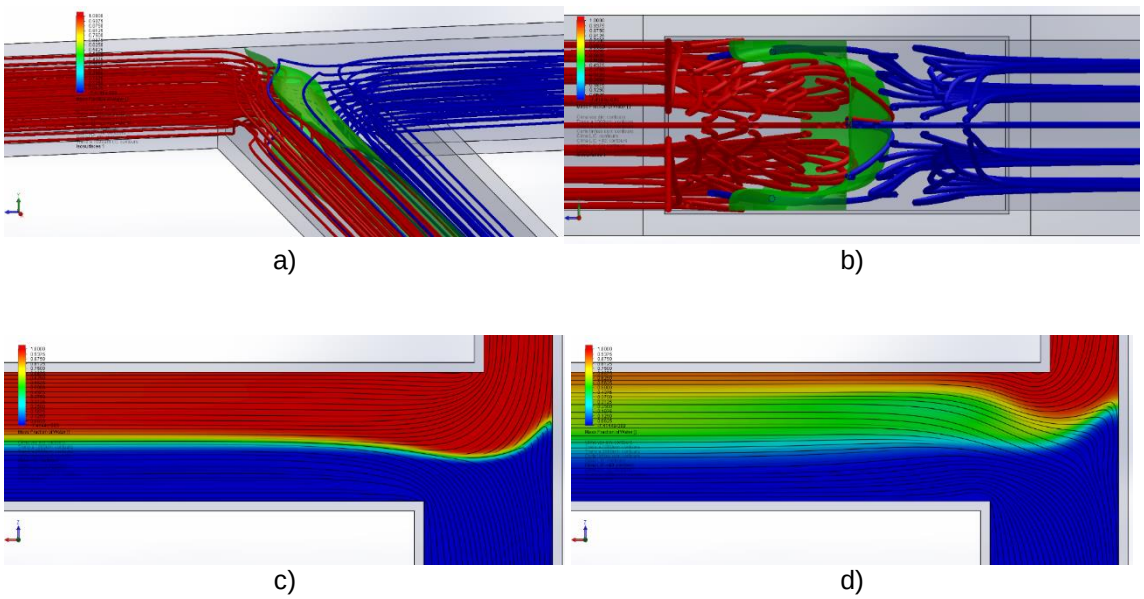

Figure 3. 7 *Representative images of the flow inside micromixer A3, the most asymmetrical, at Re=75. a) perspective view of the mixing zone, constituted by 50 tubes of each fluid and an isosurface of mass fraction of water equal to 0.5. b) view inside the entire mixing channel, constituted similarly to a). c) colour plot of the mass fraction in the middle plane between upper and bottom walls of the micromixer, with streamlines. d) colour plot of the mass fraction, but now in a plane that is 40μm above the middle one*

to penetrate the water side. On the other hand, water fluid elements are diverted from the upper planes of the mixer channel to the middle planes and into the side walls of the mixing channel. This is an evidence of the presence of advection inside the asymmetrical micromixer. Along this

regime, as the Reynolds number increases, these mechanisms become increasingly more intense, which can be confirmed by the further penetration of bromothymol into the side wall of the water stream. Looking from a more global perspective, the dominant mechanism of the mixing quality appears to be still diffusion, but now with advection also playing a role. This results in a consistent increase of the mixing quality α_{mix}.

3.2.1.3 Regime III

For the geometries studied in the present thesis, regime III develops from Re≈100 up to Re≈125. It is quite a narrow range in terms of flow, but the structures that start to unveil in this regime are of great importance for mixing.

The first feature that is possible to observe is the reaching of the water-side wall by the bromothymol in the mixing channel, creating multiple water-bromothymol interfaces, thus decreasing local characteristic lengths, improving the mixing quality of the micromixer (figures 3.8a and b). Figure 3.8c displays a recirculation zone in the water side at the channel horizontal midplane. This recirculation zone improves asymmetrical micromixers performance by allowing

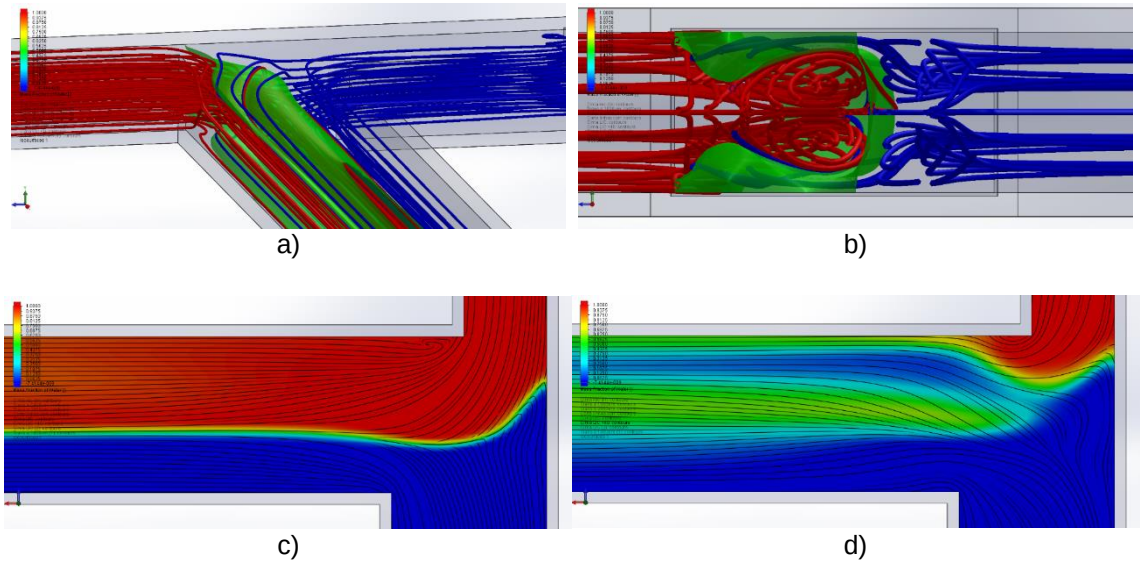

Figure 3. 8 *Representative images of the flow inside micromixer A3, the most asymmetrical, at Re=125. a) perspective view of the mixing zone, constituted by 50 tubes of each fluid and an isosurface of mass fraction of water equal to 0.5. b) view inside the entire mixing channel and it is constituted similarly to a). c) colour plot of the mass fraction in the middle plane between upper and bottom walls of the micromixer, with streamlines. d) colour plot of the mass fraction, but now in a plane that is 40μm above the middle one.*

bromothymol that flows in the vicinity to have enough time to mix with the water trapped in it.

In the mixing zone, the water-bromothymol interface is now substantially deformed, being able to guide quite well some bromothymol into its side of the mixing channel, and another fraction into the water side (by the upper and lower sides) (figure 3.8d). This bromothymol flow forms an interface that engulfs the water, as it can be seen in figures 3.8a and b, accelerating it along the mixing channel. Also, it is possible to observe the appearance of two counter-rotating vortices.

These structures form from the centrifugal forces felt by the water elements flowing in the upper and lower parts of the channel being deflected to the centre, and side wall of the mixing channel.

Downstream the mixing zone, the micromixer appears to lose symmetry (figure 3.8c). This is due to the deficit of bromothymol mass flow rate that has gone into the water site, and since there is no water going into the bromothymol side, this imbalance translates into the referred asymmetry. This lack of symmetry is also a good indicator of the amount of bromothymol flowing into the water side: the larger the mass flow rate of bromothymol is going into the water side, the wider the water side flow is. In terms of mixing mechanisms, both diffusion and advection play an important role in this regime. In the mixing zone, advection is the most important one, with the water-bromothymol interface being no longer well defined, a recirculation zone and a pair of vortices assure that locally the diffusion lengths decrease, with higher residence times. Downstream the streamlines straighten up, but with the lamellae created in the mixing zone, the characteristic diffusion lengths decrease, improving mixing quality.

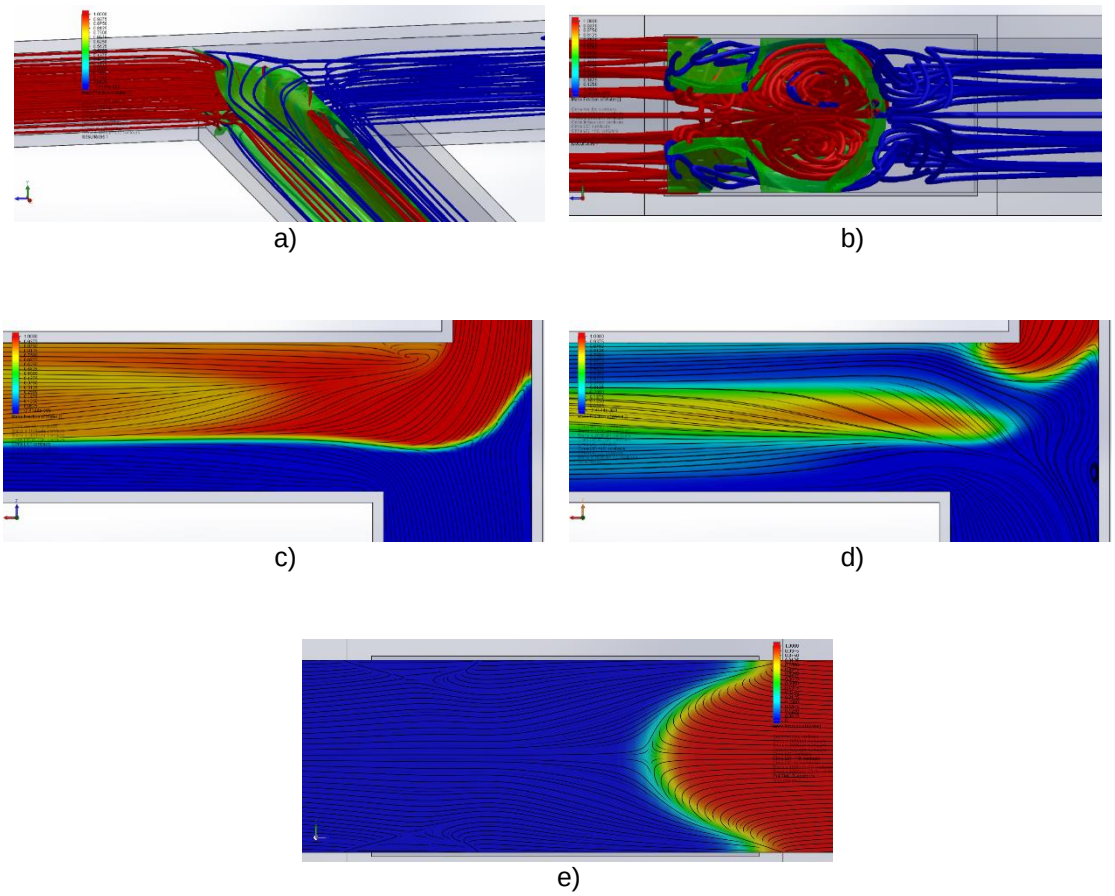

Figure 3. 9 *Representative images of the flow inside micromixer A3, the most asymmetrical, at Re=200. a) perspective view of the mixing zone, constituted by 50 tubes of each fluid and an isosurface of mass fraction of water equal to 0.5. b) view inside the entire mixing channel and it is constituted similarly to a). c) colour plot of the mass fraction in the middle plane between upper and bottom walls of the micromixer, with streamlines. d) colour plot of the mass fraction, but now in a plane that is 40μm above the middle one. Image e) cross section view of the micromixer at a distance of 6μm from the common wall, with streamlines.*

3.2.1.4 Regime IV

With the flow rates increasing, more bromothymol penetrates into the water-flow side and, as displayed in figures 3.9a and b, this flow engulfs even more the flow of water, intensifying the pair of vortices due to higher velocities and, consequently, higher centrifugal forces. On the other hand, it is now clear that on the bromothymol-flow side a new pair of counter rotating vortices has also formed but, again, with a negligible amount of water passing to the bromothymol side. Because of the dominating strength of the water-side vortices, the much less strong vortices recently formed in the bromothymol-flow side have a weak influence in the mixing process.

In Regime IV another fact becomes clear. Figure 3.9c shows a clear recirculation zone in the water side, which is not present in bromothymol side. In a similar way to the symmetric case, the two fluid streams entering the micromixer collide, inducing the conversion of kinetic energy into pressure energy. The less adverse pressure gradient induced by the increase in pressure prevents the flow separation in the 90º corner of the bromothymol side but the same does not happen in the water side. A significant recirculation zone exists due to the more intense velocity field. This phenomenon was present in Regime III, but becomes clearer in Regime IV, with the recirculation zone growing in size.

Figure 3.9c shows mixing already occurring at the horizontal midplane inside the recirculation zone (which is significantly bigger) on the water side. Above this midplane, at the upper part of the mixer, next to the wall common to both inlet channels it is now possible to see that a new vortex has formed in the bromothymol side, next to the common wall (figure 3.9d and e), in the left side). This pair of vortices has a great influence on the performance of the micromixer as it helps directing the flow of bromothymol towards the mixing channel and limits the amount that goes to the water side. Again, downstream the mixing channel, the streamlines straighten up and vortices end up dissipating, so diffusion becomes the most important mixing mechanism at play. On the other side, advection mechanisms are strongly present in the mixing zone and are responsible for most of the mixing quality, as the value for α_{mix} is twice the one for Re ≈ 25, where diffusion prevails. It should be noticed that regime IV lasts for the longest Reynolds number range; actually, the parameter α_{mix} does not increase as significantly as in regime II and III, which allows one to infer that this regime is characterized by a marked stability, partially balancing the mechanisms that accelerate or decelerate mixing, but always with an improvement as α_{mix} keeps increasing with the Reynolds number.

3.2.1.5 Regime V

Transition to regime V occurs when the pair of vortices present near the wall common to both inlets merge into a single vortex, now visible in the middle plane of the micromixer – see figure 3.10c, but shifted towards the interface water-bromothymol.

Additionally, it was possible to see the formation of a pair of vortices in the bromothymol side, near the common wall (figure 3.10e). As this happens α_{mix} starts do increase significantly, as shown in figure 3.1 (micromixer A3 and A2). While the pair of vortices identified in the previous regime shift to the middle plane and away from the inlet of bromothymol, the flow is no longer directed towards the mixing channel, going straight to the water side. As in regime II, as water fluid elements transport more momentum and kinetic energy in regime V, bromothymol fluid elements are deviated towards the upper and lower sides of the mixing channel. The influence of the pair of vortices formed in regime V induce a local constriction that accelerates the bromothymol flowing between them. As a consequence, the velocity field is strong enough for the interface between the water and bromothymol to be completely disrupted (Figure 3.10).

In the recirculation zone present near the wall of the water-side it is possible to verify that an intense mixing occurs between both fluids (note that the green colour in figure 3.10c stands for mass fraction of water equal to 0.5, which is the target value), as a consequence of bromothymol entering this zone and remaining there long enough for mixing to occur. The strong velocity field results in 3 pairs of vortices, two on the water side, and one on the bromothymol side. As in previous cases, with no water going to the bromothymol side, the two vortices present in this side have weak influence in the global performance of the micromixer.

In the water side the opposite occurs. With the interface water-bromothymol completely disrupted, figure 3.10b shows stream tubes of water entangled with stream tubes of bromothymol. This has as direct consequence an increase of the mixing in spite of the straightening up of the flow streamlines downstream the mixing channel (figure 3.10.c), since the characteristic mixing lengths are now small enough for diffusion to occur. This is also the reason why α_{mix} increases significantly with the Reynolds number. As the flow rate increases, the higher kinetic energy transported by the fluid elements will contribute to energize the vortices present, so more flow tubes will be entangled allowing for a much better mixing.

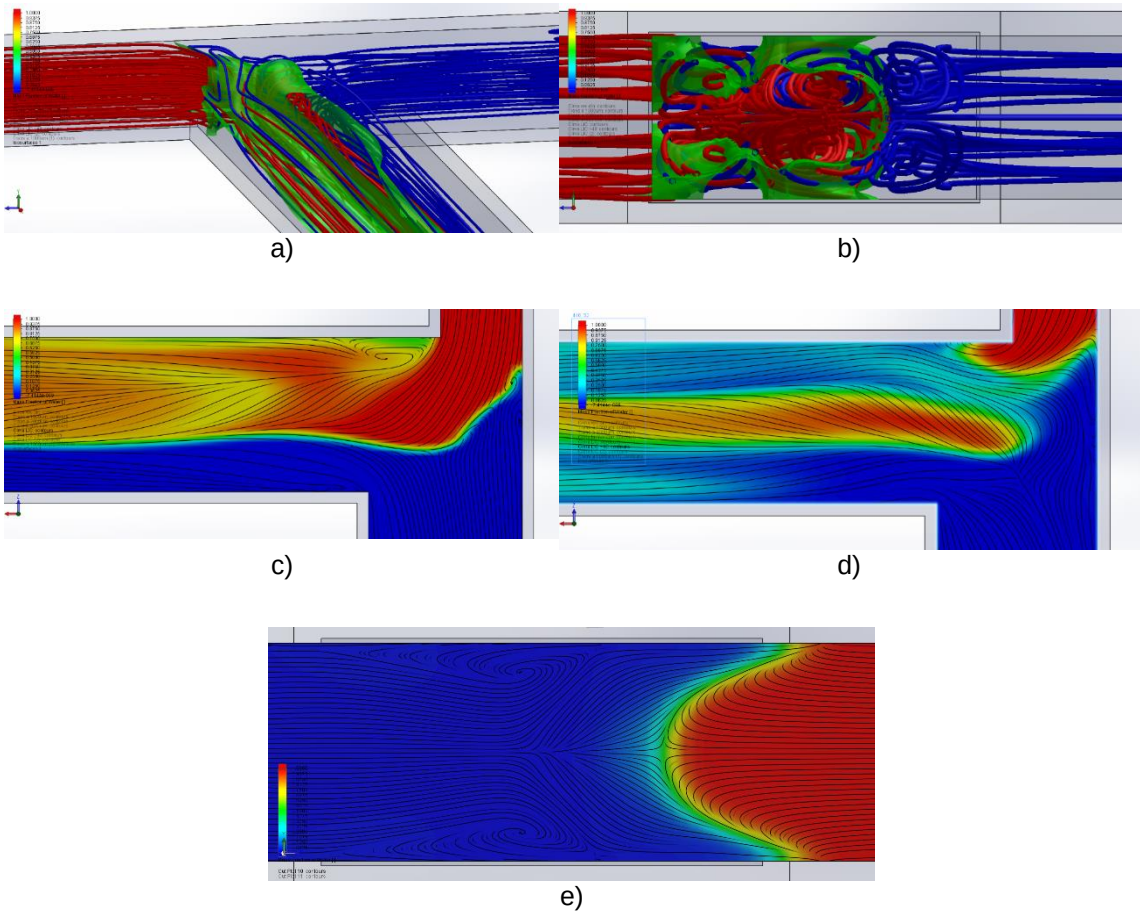

Figure 3. 10 *Representative images of the flow inside micromixer A3, the most asymmetrical, at Re=275. a) perspective view of the mixing zone, constituted by 50 tubes of each fluid and an isosurface of mass fraction of water equal to 0.5. b) view inside the entire mixing channel and it is constituted similarly to a). c) colour plot of the mass fraction in the middle plane between upper and bottom walls of the micromixer, with streamlines. d) colour plot of the mass fraction, but now in a plane that is 40μm above the middle one. Image e) show a cross section view of the micromixer at a distance of 6μm from the common wall, with streamlines.*

3.2.2. Effect of the Degree of Asymmetry

A direct analysis of figure 3.1 shows that the more asymmetrical the micromixer is, the better is the performance. This fact becomes increasingly pronounced at higher Reynolds numbers. The reason behind this is most likely the dominating role of the viscous forces at lower Reynolds numbers in the momentum balance. Such intensity of viscous forces can damp the flow perturbations that arise from geometrical differences. This justifies why regime I from

asymmetrical micromixers matches exactly the *Stratified Laminar* flow from the symmetrical micromixers.

As the Reynolds number increase and inertial forces gain relative importance, the level of asymmetry starts to become a significant parameter concerning the mixing quality. Most physical structures discussed in the previous section form because there is a difference in the momentum carried by fluid elements from both streams. The more asymmetrical the micromixer is, the bigger the difference in momentum and kinetic energy carried by both streams is and, ultimately, the better is the mixing achieved.

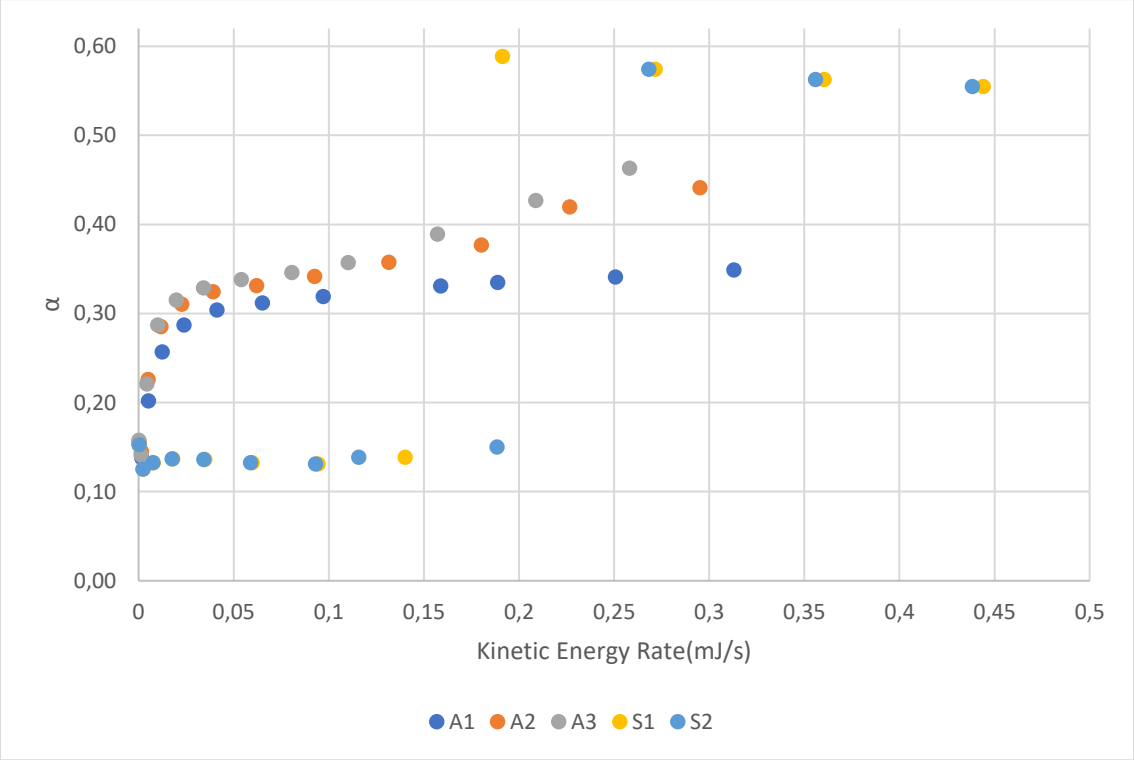

Figure 3. 11 *Plot of the mixing quality versus the kinetic energy rate at the micromixer inlets for the five studied geometries*

Observation of figure 3.11 shows that as the mass flow rate increases, the difference in kinetic energy rate between different geometries also increase. As already observed in figure 3.1, also this new perspective confirms the completely different behaviour between the symmetric and the asymmetric micromixers. When the transition from laminar vortex regime to the engulfment occurs, the flow structure changes completely and the mixing quality increases in an almost asymptotic way. In the asymmetric micromixers were identified five different flow regimes, and flow transition is smoother.

Among the asymmetric micromixers, A1 exhibits the higher values of total inlet kinetic energy rate for the same Re at the outlet channel, and the micromixer A3 exhibits the lowest total inlet kinetic energy rate. This trend is related to the more intense velocity field present at the inlets of micromixer A1, due to the lower width relative to A3. Looking from this point of view, and for the same Re in the mixing channel, as higher kinetic energy rates correspond do lower mixing quality, one can infer that the kinetic energy transported by the fluid elements represent a source of

energy that helps sustaining the existence of the vortices present in the mixing zone, which do not favour mixing.

Figure 3.12 shows the flow visualization at Re ≈ 275 inside micromixer A1, the least asymmetrical one. Figures 3.12a and b clearly shows that, despite the existence of 3 pairs of vortices in the mixing channel, just as in micromixer A3, the flow is more segregated. It is no longer possible to detect entanglement of the vortices from both fluids and there is much more bromothymol in the bromothymol side, with the respective pair of vortices looking more intense. It was concluded before that the pair of vortices from the side of the bromothymol had a weak contribution to improve the mixing of the streams; when comparing this micromixer performance with that of A3, it becomes clear that there is a performance improvement with asymmetry. By looking at figures 3.12c and d, the reason behind this poor performance of micromixer A1 compared to A3 becomes clear. At Re ≈ 275 the pair of vortices that were present near the common wall in of both streams for Re ≈ 200, merged into a single one, just as in the most asymmetrical micromixer. However, in the present case, this vortex is present along the whole height of the geometry, in opposition to that occurring in micromixer A3 where this vortex appears only in the vicinity of the middle plane and moved towards the water-bromothymol interface, allowing the formation of another pair of vortices parallel to the axis of the mixing channel. This happens because the kinetic energy rate transported by the fluid elements is not high enough to energize the merge of the pair of vortices into a single one as occurring in A1. In micromixer A1, this vortex directs more bromothymol to its side in the mixing channel, and the amount that manages to penetrate into the water side is not enough to disrupt the interface, and the flow remains in regime IV.

Globally, in the less asymmetrical micromixer A1 the most important mixing mechanism present is still advection, and the very intense vortices formed confirm it. The main differences comparing to the more asymmetrical micromixers are related to the non-disruption of the water-bromothymol interface; because of that, downstream the mixing zone the mixing characteristic lengths are not short enough for diffusion to occur efficiently when the vortices dissipate, and the streamlines straighten. In the more asymmetrical micromixers, as seen before, the complete disruption of the water-bromothymol interface resulted a significant increase in the advection mechanisms. Also, that allowed the appearance of more water-bromothymol interfaces, and consequently the reduction of the characteristic lengths for diffusion to occur downstream. Both mechanisms gave an important contribution for a significantly higher value of α_{mix}.

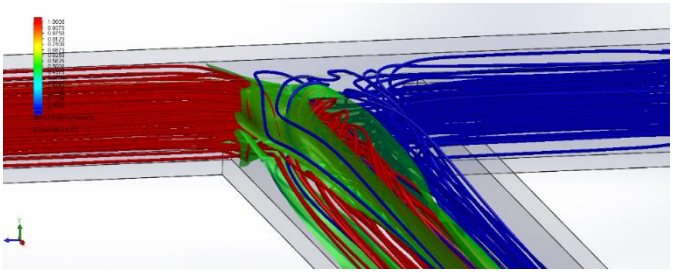

a)

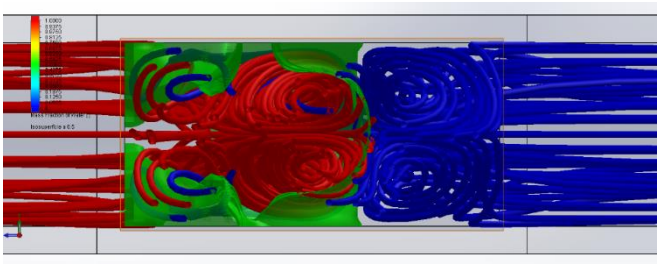

b)

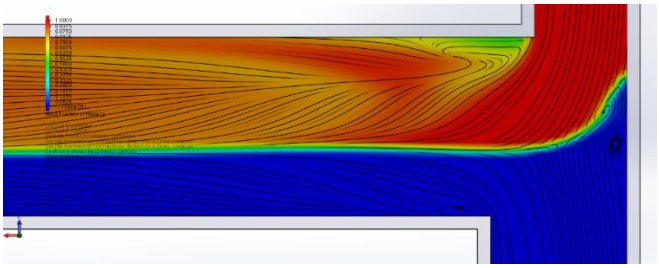

c)

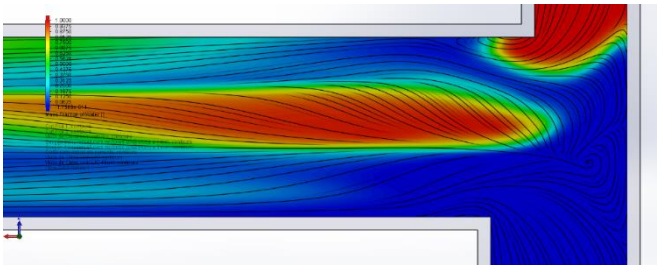

d)

Figure 3. 12 *Images of the flow inside micromixer A1, the least asymmetrical, at Re=275. a) perspective view of the mixing zone, constituted by 50 tubes of each fluid and an isosurface of mass fraction of water equal to 0.5. b) view inside the entire mixing channel and it is constituted similarly to a). c) colour plot of the mass fraction in the middle plane between upper and bottom walls of the micromixer, with streamlines. d) colour plot of the mass fraction, but now in a plane that is 40μm above the middle one.*

Chapter 4- Conclusions and Suggestions for Future Work

4.1 Conclusions

One of the major challenges in the field of microfluidics is the development of technologies and methods capable of efficiently promote mixing between fluids, due to the strong dominance of the surface effects over inertial ones, which delay the transition from laminar regime that is characterized by better mixing capabilities. In the 90's of the previous century, the development of LOC (Lab-On-A-Chip) and μ-TAS devices led to significant developments in chemical, biological and biochemical experiments, with high waste reduction, and reduced energy consumption and costs, but with the fundamental problems associated with flows at low Reynolds numbers still to be efficiently solved. With the requirement of high mixing times and lengths for fluid mixing to occur at the scale of those devices, the development of new chips, capable of achieving better mixing, is needed. Among all the types of micromixers developed, T-shaped micromixers, having a simple geometry and being easy to integrate into μ-TAS applications, stands out.

It is within this scope that this thesis was done. In fact, the main objectives of the present work are, on one side the detailed characterization by CFD of the flow regimes that develop inside T-shaped micromixers according to inlet geometrical and operation conditions and, on the other side, the physical analysis of the flows inside these devices for each regime. The conclusions drawn from this work will allow a better understanding of how the degree of geometrical asymmetry together with the mass flow rate maximize mixing quality.

To accomplish the objectives, five different T-micromixer geometries were numerically modelled: three asymmetrical geometries with different degrees of asymmetry and two symmetrical geometries; one with perfect ninety-degree corners into the mixing channel, and one with round corners into the mixing channel similar to the ones used in experimental works. Mixing between two similar fluids flowing through both inlets was studied. A total of 12 simulations were performed for each geometry, using Reynolds numbers (based on the mass flow rate at the micromixer outlet) in the range 25 - 300. At one of the inlets water was introduced into the T-micromixer, whereas at the other inlet an aqueous solution of bromothymol entered the T-micromixer. At each inlet, the same mass flow rate was imposed. This ensures that the only asymmetry analysed was geometrical.

To evaluate the mixing efficiency of the micromixers, two parameters were used. One is based on the state of segregation of the flow, which has been widely used by other authors in the literature. The other parameter, which is a novel approach, aims at relating the kinetic energy rates at both the inlets of the micromixer with the degree of asymmetry.

The numerical simulations results allowed for flow visualisations to facilitate the physical analysis. Regarding the symmetrical case, and as expected from other authors' works reported in the literature, three different regimes were clearly identified. First the stratified laminar regime, characterized by straight parallel streamlines in the mixing channel, the fluids being separated by a defined interface (a segregated flow occurring up to Re ≈ 50), with only molecular diffusion acting as the mixing mechanism. From around Re ≈ 50 onwards, two pairs of counter rotating vortices form in the mixing zone, together with a pair of vortices in the common wall to both streams of fluids. As the first pair of vortices forms due to the centrifugal forces experienced by fluid elements entering the mixing channel, the second one forms due to the local adverse pressure gradient resulting from the presence of a stagnation point where both streams meet. Both fluid streams remain separated by a defined interface. At Re ≈ 225, there is an abrupt change in the flow configuration. It is the transition to the engulfment regime, characterized by strong advection in the mixing zone caused the break-up of the interface separating both fluids, and the entanglement of these. The two pairs of counter rotating vortices formed collapsed into two vortices, with great mixing capacity. Despite downstream the micromixer junction the streamlines straighten up, the flow is structured as small lamellae that reduce the characteristic lengths and boost diffusion mixing.

Comparison between the geometry with perfect ninety-degree corners and the one with smoothed out corners shows that geometrical imperfections delay the transition to the engulfment regime, which agrees with the experimental tests. Additionally, numerical simulations predicted a significantly higher mixing quality in the engulfment regime, comparing to the values obtained from experimental tests. This difference is justified by the fact that α_{mix} is experimentally obtained from acquired images taken from microscope observation, at approximately middle plane of the micromixer. Not only there is no guaranty that the results are not influenced by adjacent planes (lens focus not at the midplane as intended), but also noise introduced by the camera influence the results, even with subsequent digital treatment of the images. As images from the experimental work show close similarities with the ones taken from the numerical simulations, the difference in the mixing quality may be related with the experimental error inherent to the previous works.

For the asymmetrical micromixers, the numerical simulations allowed for the identification, and characterization, of five different regimes. Regime I (up to Re ≈ 50) is very similar to the stratified laminar regime observed in the symmetrical case, with both streams completely segregated by a defined interface, parallel streamlines, and only molecular diffusion acting as the mixing mechanism. At Re ≈ 50 transition to regime II occurs. It is already possible to observe the passage of bromothymol (that transports less linear momentum) to the water side, deflected to the upper and lower walls of the micromixer by centrifugal forces. This flow pattern is the first evidence of the presence of advection as mixing mechanism, despite the greater relative importance that molecular diffusion still has. Regime III, identifiable in the Reynolds number range of around 100 to 125, is characterized by the fact that the bromothymol solution has already

reached the water side wall and entered the recirculation zone formed as a consequence of the local adverse pressure gradient (and flow separation) induced by the ninety-degree corner of the water side. Also, a pair of vortices form in the water side. At this point, advection is the main mixing mechanism in the mixing zone. For regime IV, in the Reynolds number range of 125-225, it is possible to observe the appearance of a new pair of vortices next to the common wall that helps directing the bromothymol solution towards the mixing channel. As this structure limits the water going directly into the water side of the mixing channel, this regime is characterized by a stabilization of the mixing quality parameter, although this parameter keeps increasing energized by the higher mass flow rates. From Re ≈ 225 onwards, in regime V, the pair of vortices formed before merge and shift towards the water side. Consequently, this regime is characterized by the total disruption of the water-bromothymol segregation and the presence of three pairs of vortices, with great entanglement of water streamlines with those of the bromothymol ones. Advection is the main mixing mechanism present in this regime.

In terms of geometry, results show that the more asymmetrical the micromixer is, the better is the performance (*i.e.* the larger is the mixing parameter). This behaviour can be explained by the difference in the transported kinetic energy rate between both inlets. The smaller the asymmetry is, the smaller is the kinetic energy rate transported by each fluid flow at the inlets, and more kinetic energy is converted into pressure energy. The higher kinetic energy transported through the inlets in the least asymmetrical micromixer helps sustaining the existence of vortices in the mixing zone, which can be confirmed by the presence of an additional vortex that directs bromothymol into the water side, resulting in a smaller mixing quality. The symmetrical micromixer showed the best performance among all the geometries modelled from Re≈225 onwards. But as the physical mechanisms involved are completely different to the ones identified in the asymmetric micromixers, these two types of T-micromixers need do be analysed separately.

As conclusion, the initial objectives can be considered as accomplished. The results show a high consistency with the ones obtained in the experimental works in which the present thesis is based on, and allowed a detailed characterization of the flow inside asymmetrical T-micromixers, with identification of the physical mechanisms and structures involved, and how they are influenced by variations in mass flow rate and degree of asymmetry. The most asymmetrical micromixer showed the best performance in the Reynolds number range of 50 to 225. At higher Reynolds numbers the symmetric micromixer achieve better mixing quality. When transition to engulfment regime occurs, there is entanglement of both fluid streams, with passage of both fluids to the opposite side. In the asymmetric micromixers there is a portion of the fluid from the larger side that does not participate in the mixing. The introduction of the kinetic energy rate proved useful in the understanding of how the asymmetry influences mixing quality.

4.2 Suggestions for Future Work

As suggestions of future work, further conclusions can be obtained by considering a higher Reynolds number range, and also a higher number of micromixers. Despite the three geometries allowed to withdraw most relevant conclusions, the difference in the degree of asymmetry between them is not too severe. So, more geometries, with a wider range of asymmetries would allow the confirmation of the trends observed, and possibly new ones to be obtained. As the asymmetrical geometries revealed to be so promising, it would also be interesting to try other kinds of asymmetry, namely asymmetrical flow rates at the inlets, pulsed flows, and combinations between these.

Finally, a study based in the way pressure varies from the inlets to the outlet would also clarify the influence of this parameter in the sustainability of vortices inside the micromixers, if high pressure zones are consistent with reduction in the kinetic energy rate, and consequently the impact in the mixing quality.

References

1. Silva JP. Micromisturadores do tipo T de simetria variável: Caracterização experimental da mistura de fluidos Newtonianos em escoamentos pulsados. Master's thesis. Instituto Superior Técnico. 2016.
2. Calado B. Caracterização experimental da mistura de fluidos Newtonianos em microcomponentes de geometria do tipo-T assimétricos. Master's thesis. Instituto Superior Técnico. 2014.
3. Han Q, Bradshaw EM, Nilsson B, Hafler DA, Love JC. Multidimensional analysis of the frequencies and rates of cytokine secretion from single cells by quantitative microengraving. Lab on a Chip 2010;10(11):1391-1400. doi:10.1039/b926849a
4. Manz A, Graber N, Widmer HM. Miniaturized total chemical analysis systems: a novel concept for chemical sensing. Sensors and Actuators B: Chemical 1990;1(1-6):244-248. doi:10.1016/0925-4005(90)80209-i
5. Jeong GS, Chung S, Kima CB, Lee SH. Applications of mixing technology. The Analyst 2010;135:460–473. doi:10.1039/b921430e
6. Connelly JT, Kondapali S, Skoupi M, Parker JSL, Kirby BJ, Baeumner AJ. Micro-total analysis system for virus detection: microfluidic pre-concentration coupled to liposome-based detection. Anal Bioanal Chemistry 2012;402:315–323. doi:10.1007/s00216-011-5381-9
7. Capretto L, Cheng W, Hill M, Zhang X. Micromixing within microfluidic devices. Topics in Current Chemistry 2011;304:27–68. doi:10.1007/128_2011_150
8. P. Tabeling. Introduction to Microfluidics. Oxford University Press, 2005.
9. S. Hardt and F. Schönfeld. Microfluidic Technologies for Miniaturized Analysis Systems. Springer Science & Business Media, 2007
10. de Brederode V. Fundamentos de Aerodinâmica Incompressível. Autor's Edition; 1997.
11. White F. Fluid Mechanics. 6th ed. New York, NY:McGraw-Hil; 2008.
12. Dreher S, Kockmann N, Woias P. Characterization of laminar transient flow regimes and mixing in T-shaped micromixers. Heat Transfer Engineering 2009;30(1–2):91–100. doi:10.1080/01457630802293480
13. Socolofsky SA, Jirka GH. Special topics in mixing and transport processes in the environment. Engineering–Lectures. 5th ed. College Station, TX:Texas A&M University; 2005.
14. Mansur EA, Ye M, Wang Y, Dai Y. A state-of-the-art review of mixing in microfluidic mixers. Chinese Journal of Chemical Engineering 2008;16(4):503-516. doi:10.1016/s1004-9541(08)60114-7
15. Hirsch C. Numerical Computation of Internal and External Flows. Volume 1 - Fundamentals of Computational Fluid Dynamics. 2nd ed. Oxford, England:Butterworth-Heinemann; 2007.
16. Bruus H. Theoretical microfluidics - Lecture notes. 2nd ed. Autor's Edition. 2005.
17. Bothe D, Stemich C, Warnecke HJ. Fluid mixing in a T-shaped micro-mixer. Chemical Engineering Science 2006 61:2950 – 2958. doi:10.1016/j.ces.2005.10.060

18. Lomax H, Pulliam TH, Zingg DW. Fundamentals of Computational Fluid Dynamics. 1st ed. Berlin, Germany:Springer; 2001.
19. Basavarajappa M. Experimental investigation and characterization of mixing in a T-channel mixer for asymmetric inlet conditions. PhD Thesis. The University of Utah. 2012.
20. Nguyen NT, Wu Z. Micromixers—a review. Journal of Micromechanics and Microengineering 2005;15:R1–R16. doi:10.1088/0960-1317/15/2/R01
21. Engler M, Kockmann N, Kiefer T, Woias P. Numerical and experimental investigations on liquid mixing in static micromixers. Chemical Engineering Journal 2004;101:315–322. doi:10.1016/j.cej.2003.10.017
22. Silva JP, dos Santos A, Semião V. Experimental characterization of pulsed Newtonian fluid flows inside T-shaped micromixers with variable inlets widths. Experimental Thermal and Fluid Science 2017;89:249–258. doi:10.1016/j.expthermflusci.2017.08.01
23. Calado B, dos Santos A, Semião V. Characterization of the mixing regimes of Newtonian fluid flows in asymmetrical T-shaped micromixers. Experimental Thermal and Fluid Science 2016;72:218–227. doi:10.1016/j.expthermflusci.2015.11.010
24. Hsieh SS, Lin JW, Chen JH. Mixing efficiency of Y-type micromixers with different angles. International Journal of Heat and Fluid Flow 2013;44:130-139. doi:10.1016/j.ijheatfluidflow.2013.05.011
25. Andreussi T, Galletti C, Mauri R, Camarri S, Salvetti MV. Flow regimes in T-shaped micro-mixers. Computers and Chemical Engineering 2015;76:150–159. doi:10.1016/j.compchemeng.2015.02.017
26. Unger MA, Chou HP, Thorsen T, Scherer A, Quake SR. Monolithic microfabricated valves and pumps by multilayer soft lithography. Science 2000;288:113-116. doi:10.1126/science.288.5463.113
27. Gravesen P, Branebjerg J, Jensen OS. Microfluidics-a review. Journal of Micromechanics and Microengineering 1993;3:168-182.
28. Kirby BJ. Micro-and Nanoscale Fluid Mechanics: Transport in Microfluidic Devices. 1st ed. New York, NY:Cambridge University Press; 2010.
29. Hoffmann M, Schlüter M, Räbiger N. Experimental investigation of liquid–liquid mixing in T-shaped micro-mixers using µ-LIF and µ-PIV. Chemical Engineering Science 2006;61:2968 – 2976. doi:10.1016/j.ces.2005.11.029
30. Thomas S, Ameel TA. An experimental investigation of moderate Reynolds number flow in a T-Channel. Exp Fluids 2010;49:1231–1245. doi:10.1007/s00348-010-0863-7
31. Ouellette J. A new wave of microfluidic devices. Industrial Physicist 2003, 9(4):14–17.
32. Miranda JM, Oliveira H, Teixeira JA, Vicente AA, Correia JH, Minas G.Numerical study of micromixing combining alternate flow and obstacles. Heat and Mass Transfer 2010;37:581–586. doi:10.1016/j.icheatmasstransfer.2010.01.012
33. Oh KW, Ahn CH. A review of microvalves. Journal of Micromechanics and Microengineering 2006;16:R13–R39. doi:10.1088/0960-1317/16/5/R01

34. Soleymani A, Kolehmainen E, Turunen I. Numerical and experimental investigations of liquid mixing in T-type micromixers. Chemical Engineering Journal 2008;135S:S219–S228. doi:10.1016/j.cej.2007.07.048
35. Poole RJ, Alfateh M, Gauntlett AP. Bifurcation in a T-channel junction: Effects of aspect ratio and shear-thinning. Chemical Engineering Science 2013;104:839–848. doi:10.1016/j.ces.2013.10.006
36. Wong SH, Ward MCL, Wharton CW. Micro T-mixer as a rapid mixing micromixer. Sensors and Actuators B 2004;100:359-379. doi:10.1016/j.snb.2004.02.008
37. SOLIDWORKS Technical Reference - Flow Simulation. Dassault Systems; 2017
38. Arampatzis G, Assimacopoulos D. Treatment of numerical diffusion in strong convective flows. International Journal For Numerical Methods In Fluids 1994;18:313-331. doi:10.1002/fld.1650180306
39. Freziger JH, Perić M. Computational methods for fluid dynamics. 3rd ed. Berlin, German: Springer; 2002.
40. Patankar SV. Numerical heat transfer and fluid flow. United States of America: Hemisphere Publishing Corporation; 1980.
41. Roache PJ. Verification and validation in computational science and engineering. Albuquerque, New Mexico: Hermosa Publishers, 1998
42. Kockmann N, Kiefer T, Engler M, Woias P. Convective mixing and chemical reactions in microchannels with high flow rates. Sensors and Actuators B 2006;117:495–508. doi:10.1016/j.snb.2006.01.004
43. Ansari MA, Kim KY, Anwar K, Kim SM. Vortex micro T-mixer with non-aligned inputs. Chemical Engineering Journal 2012;181–182:846–850. doi:10.1016/j.cej.2011.11.113
44. Kockmann N, Engler M, Föll C, Woias P Liquid mixing in static micro mixers with various cross sections. 1st International Conference on Microchannels and Minichannels:911-918, 2003. doi:10.1115/icmm2003-1121

Appendix

Additional images of the flows inside the modelled micromixers

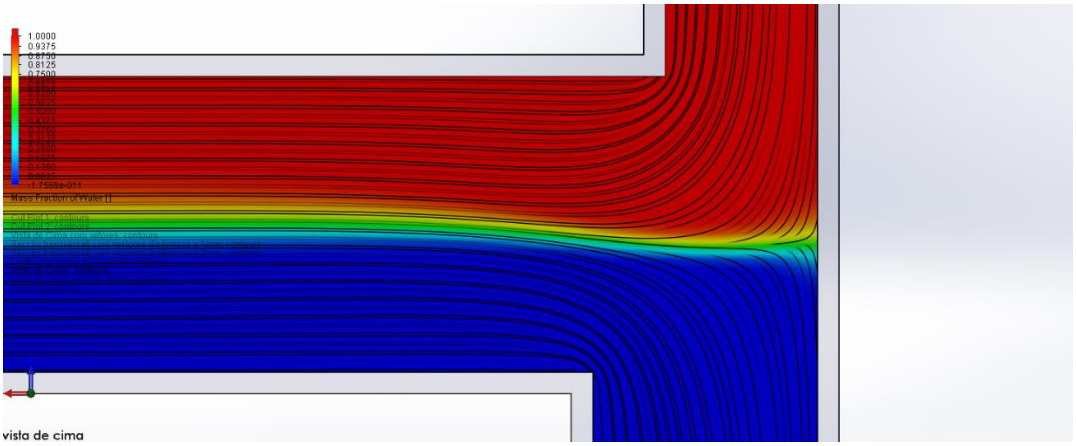

a)

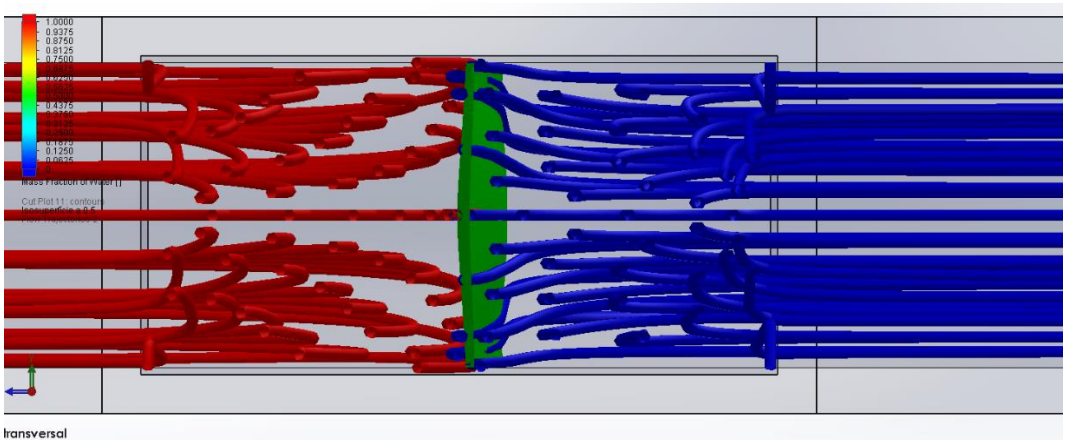

b)

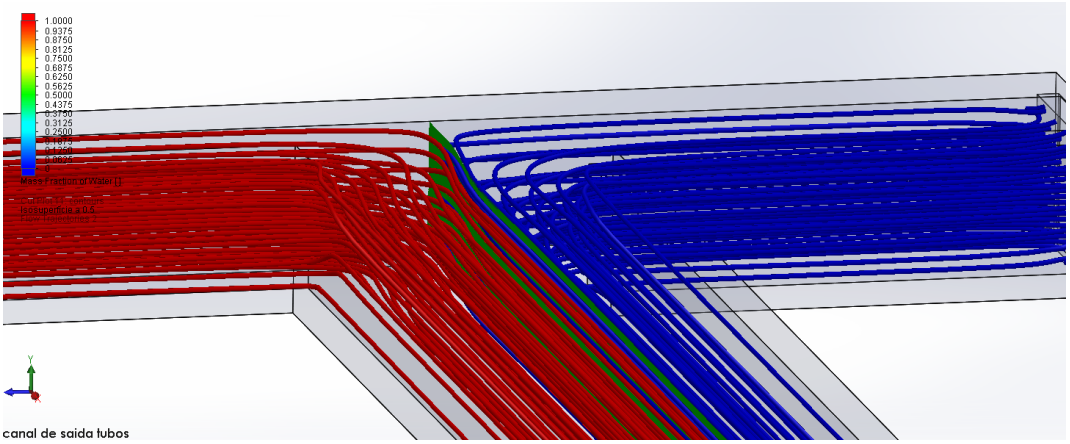

c)

Figure A 1. Images of the flow inside A1 at Re=25

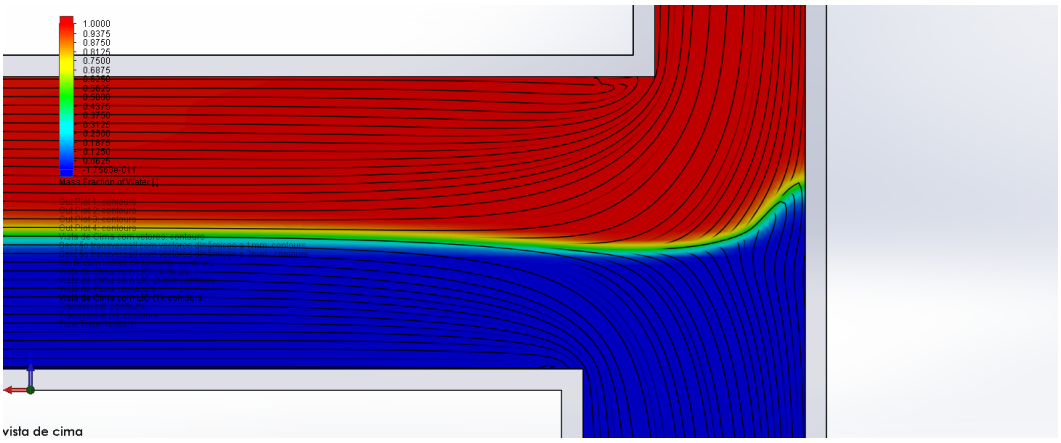

a)

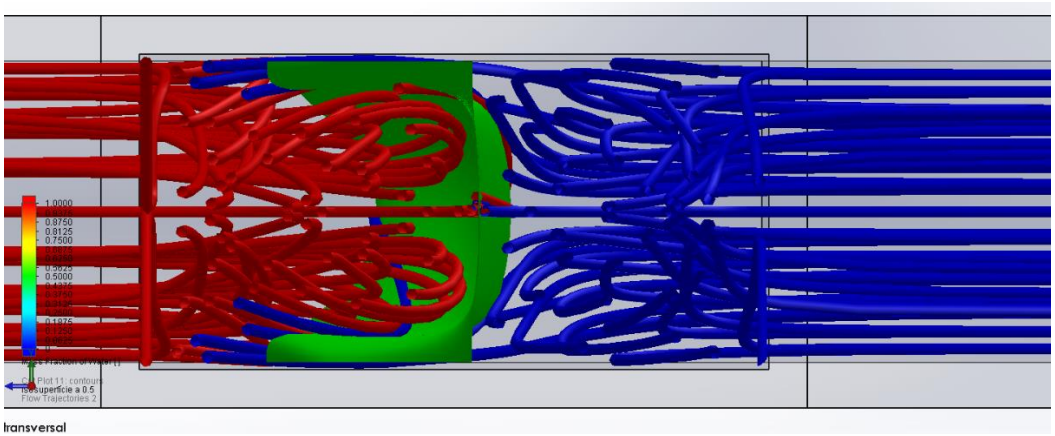

b)

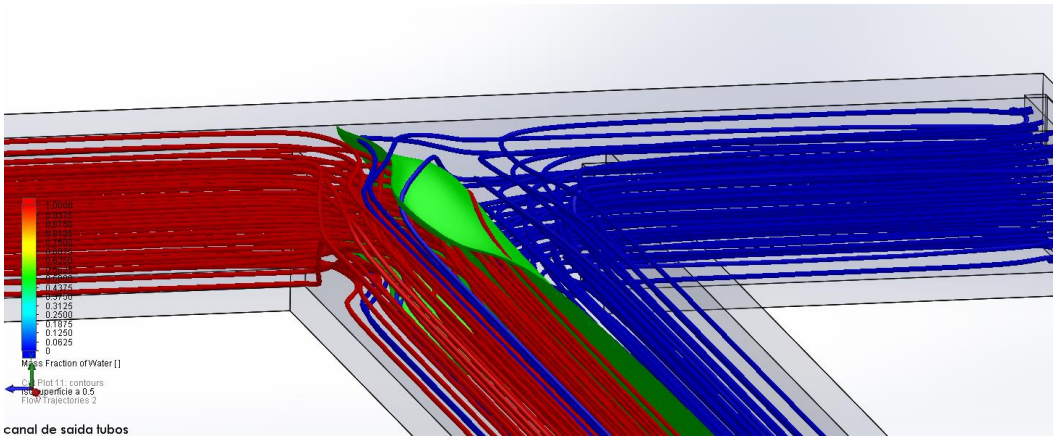

c)

Figure A 2. Images of the flow inside A1 at Re=75

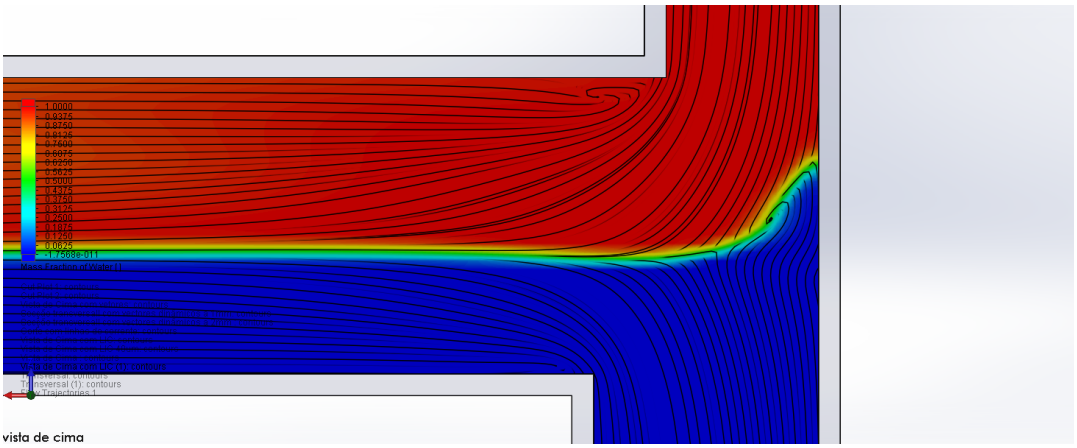

a)

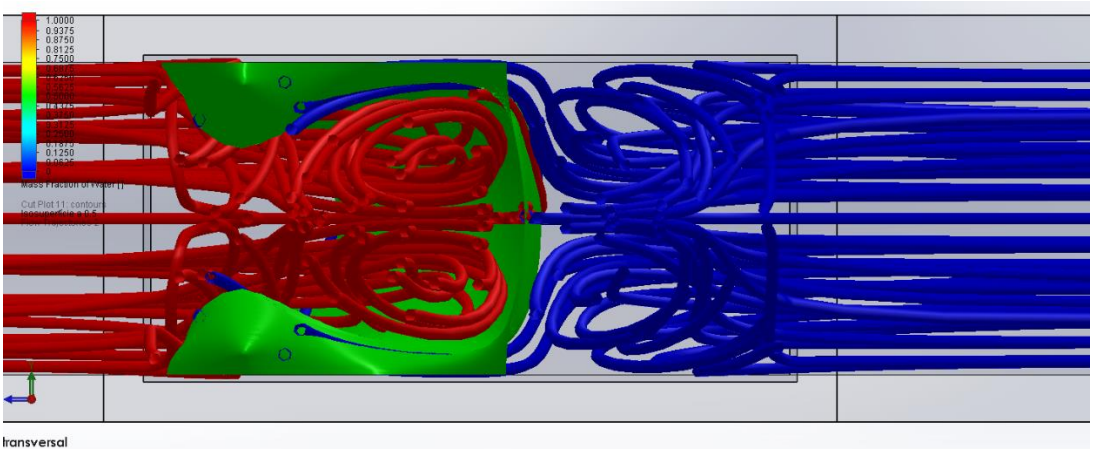

b)

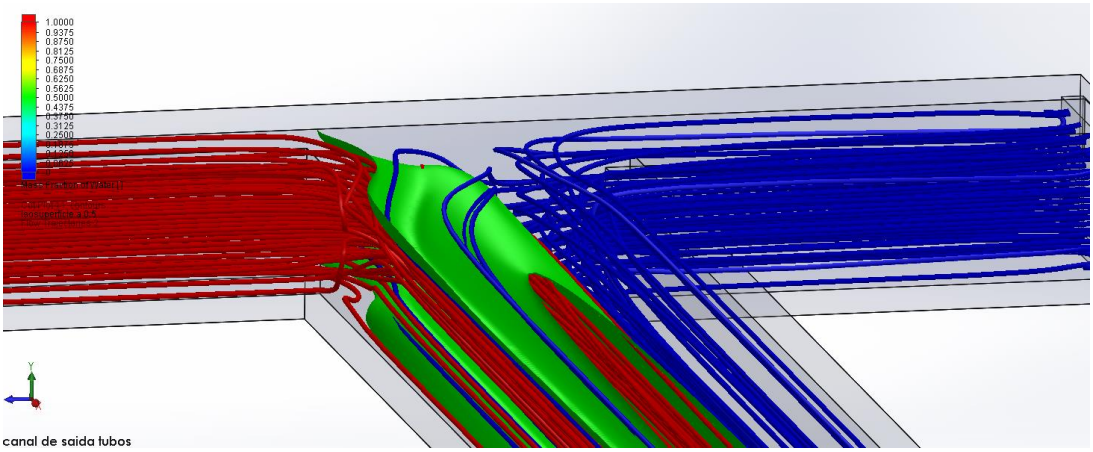

c)

Figure A 3. Images of the flow inside A1 at Re=125

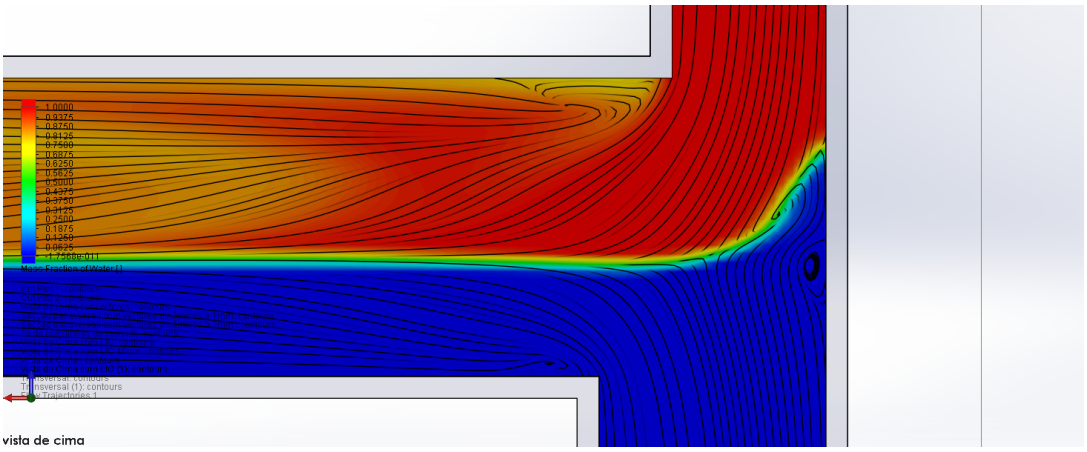

a)

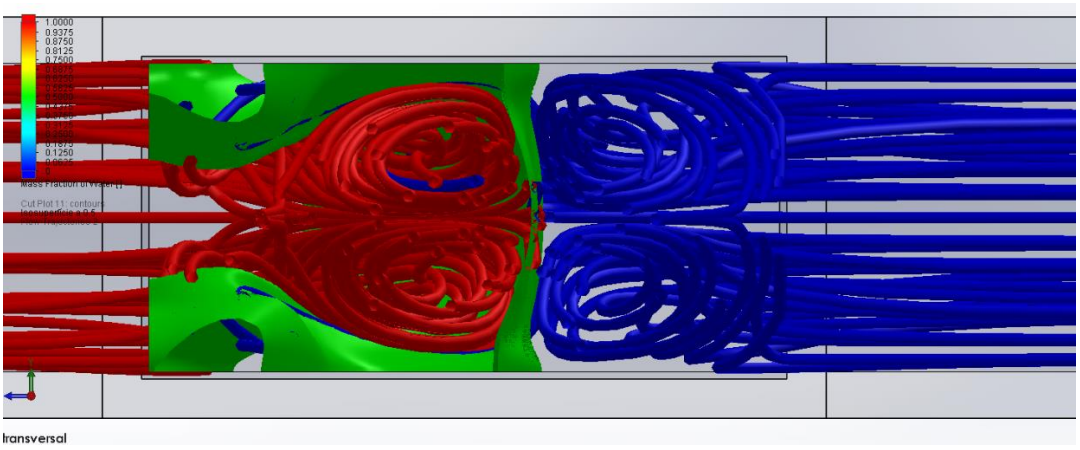

b)

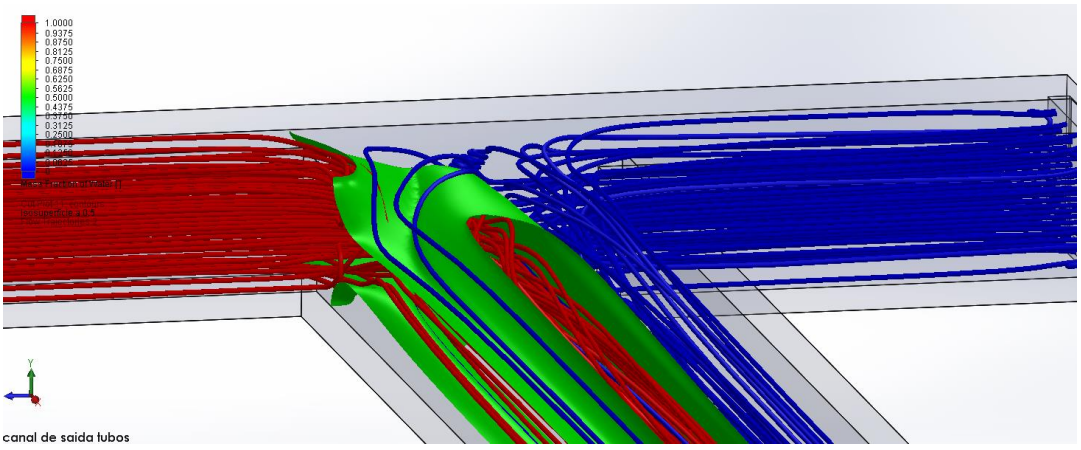

c)

Figure A 4. Images of the flow inside A1 at Re=200

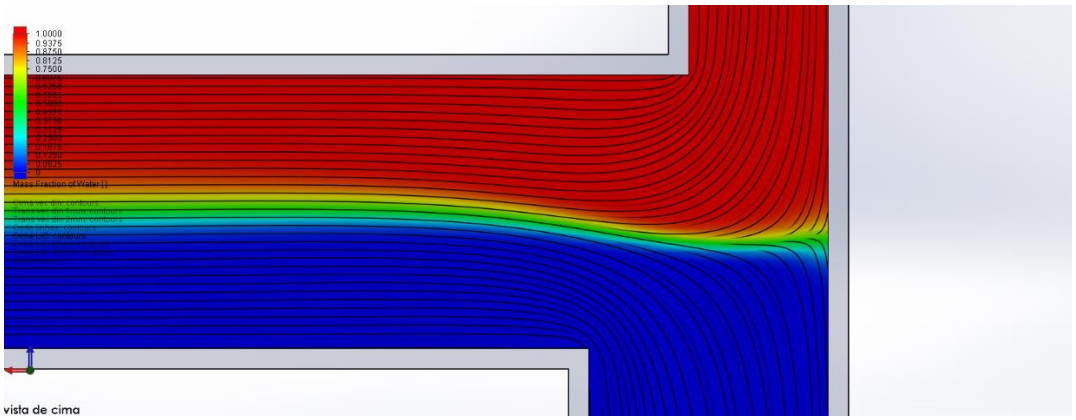

a)

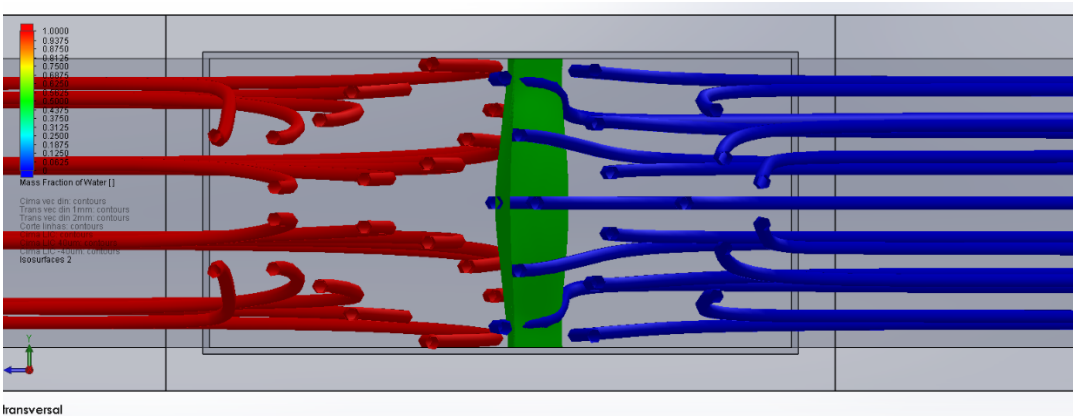

b)

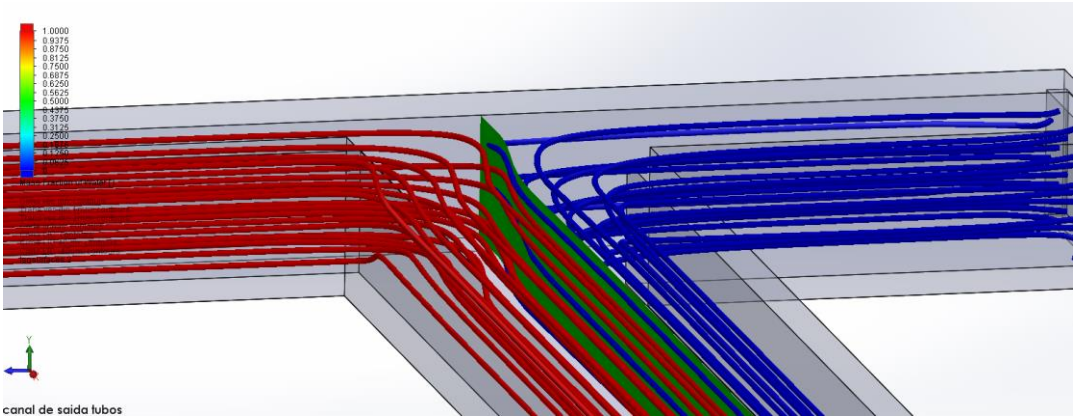

c)

Figure A 5. Images of the flow inside A2 at Re=25

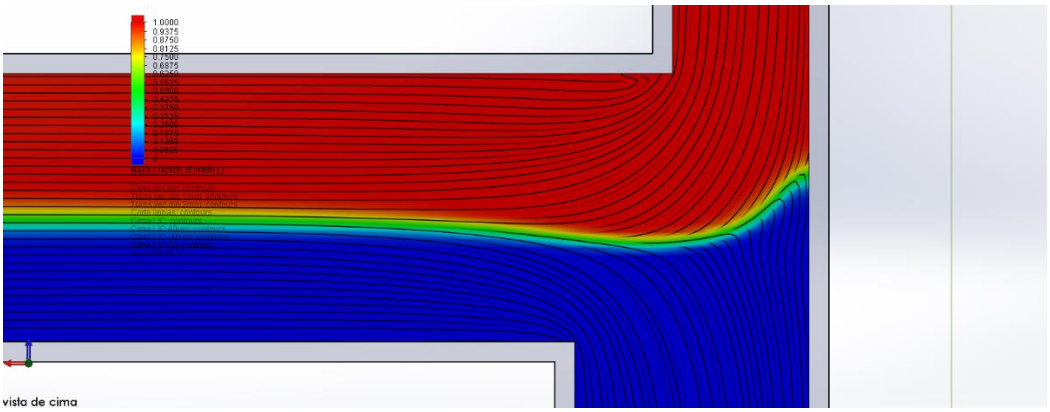

a)

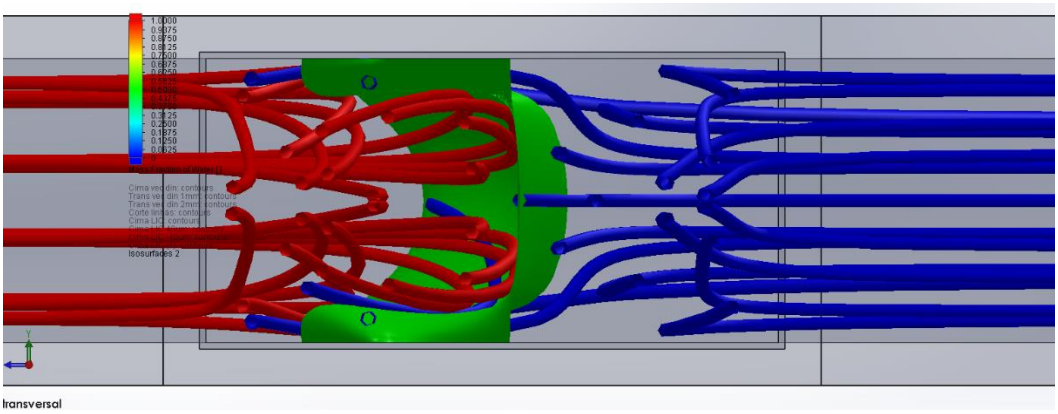

b)

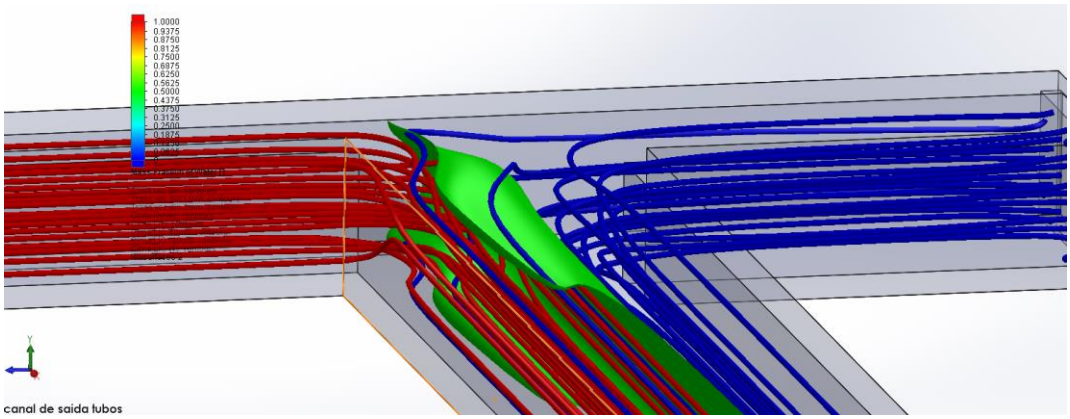

c)

Figure A 6. Images of the flow inside A2 at Re=75

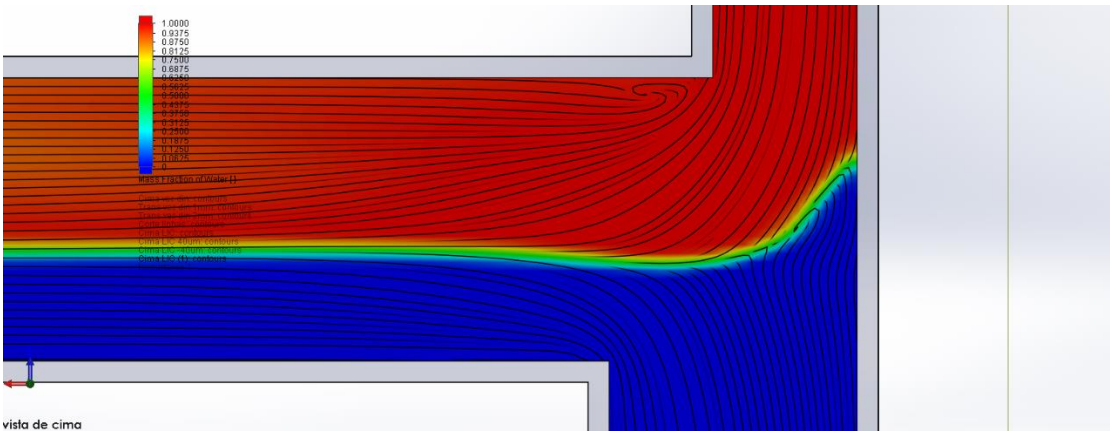

a)

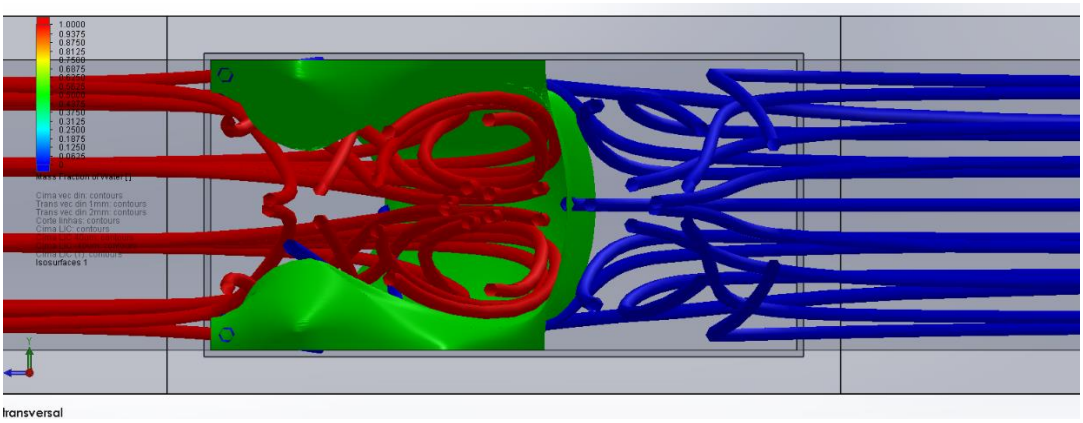

b)

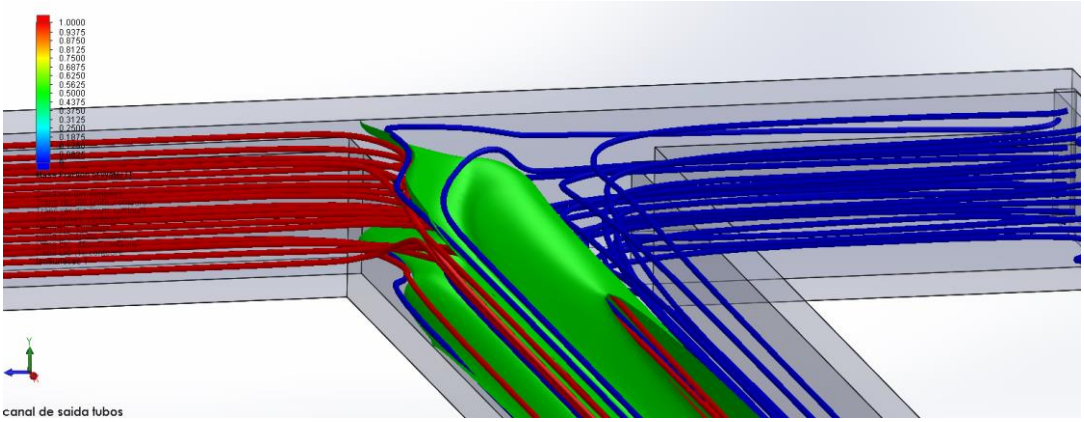

c)

Figure A 7. Images of the flow inside A2 at Re=125

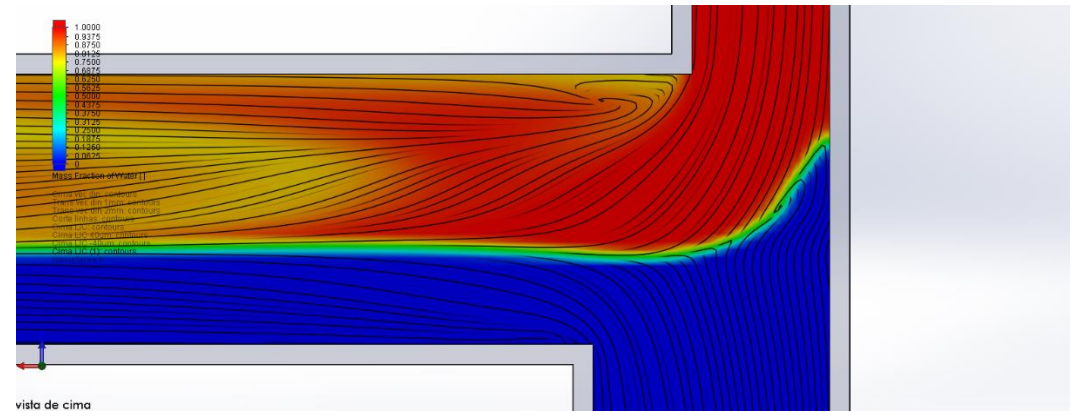

a)

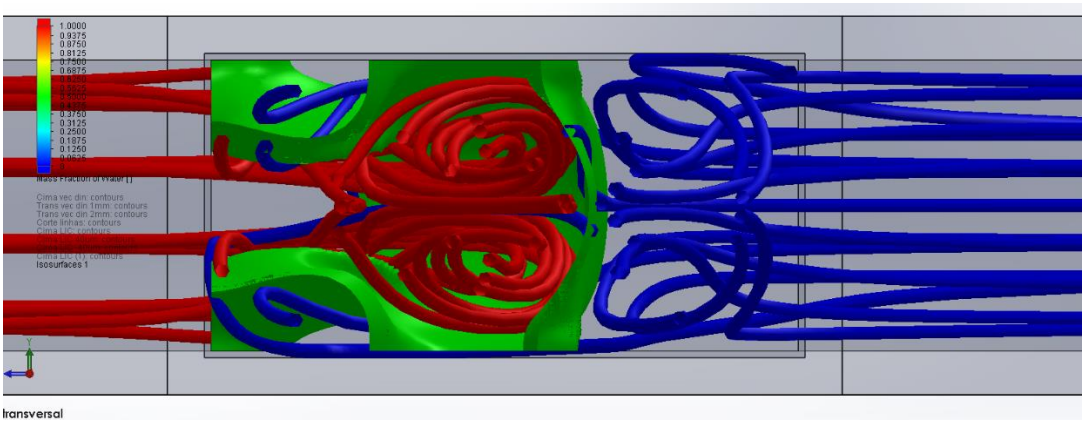

b)

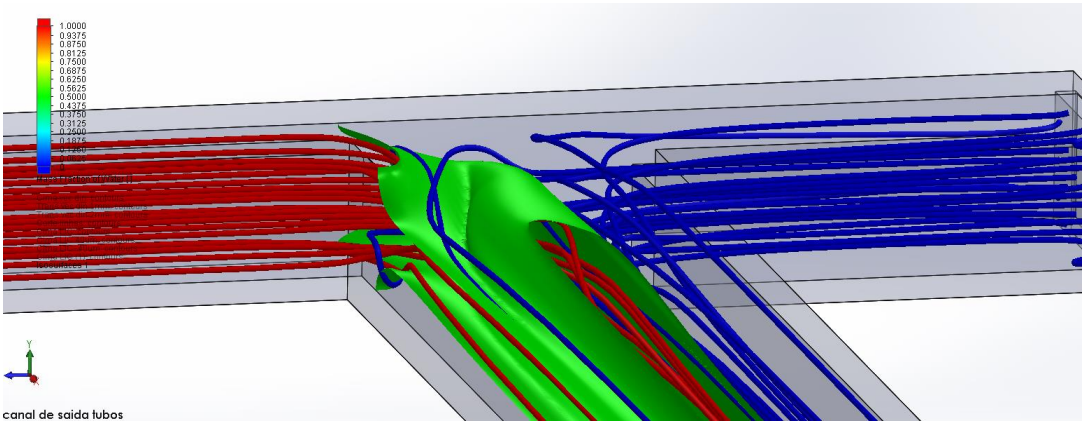

c)

Figure A 8. Images of the flow inside A2 at Re=200

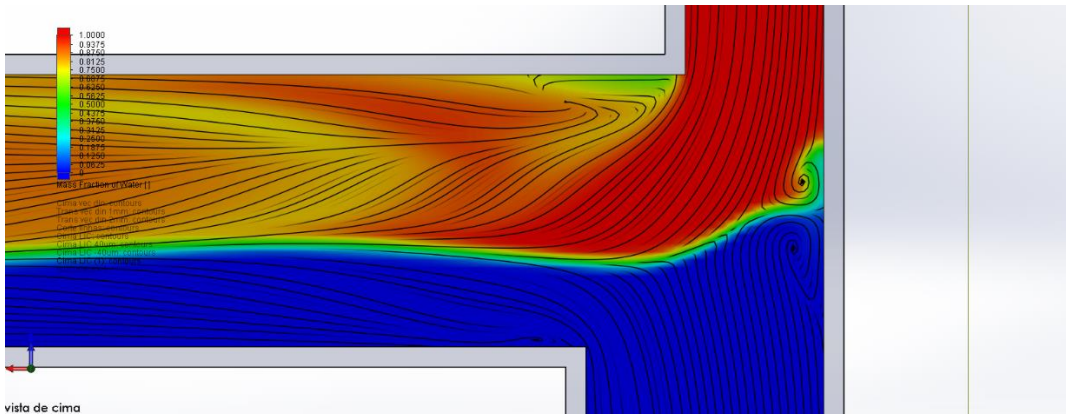

a)

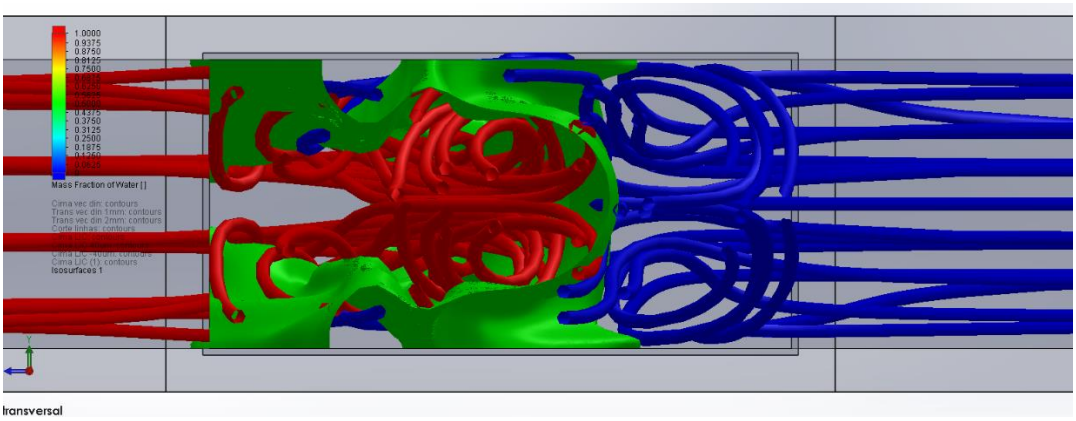

b)

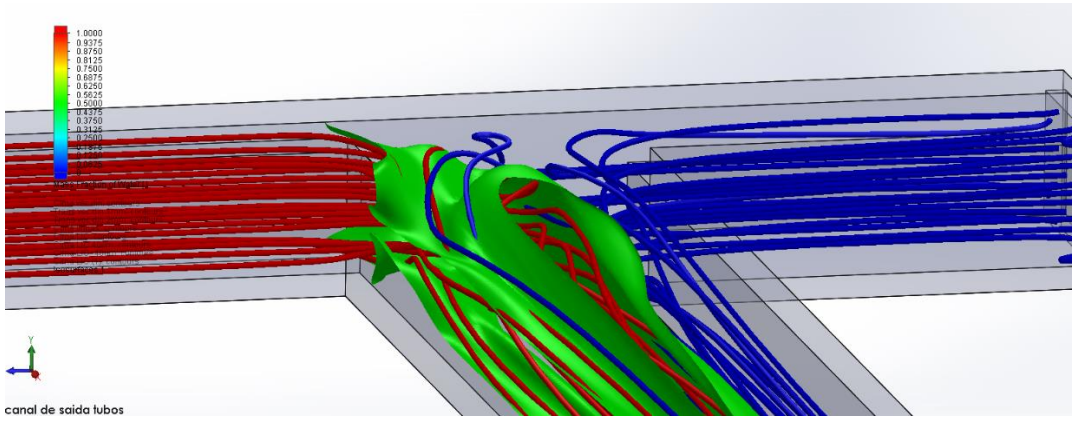

c)

Figure A 9. Images of the flow inside A2 at Re=270